The dynamics of gas bubbles in conduits of vascular plants and implications for embolism repair

W. Konrad, A. Roth-Nebelsick*

Institut für Geowissenschaften, Sigwartstrasse 10, D-72076 Tübingen, Germany

Abstract

Pressure-induced tensions in the xylem, the water conducting tissue of vascular plants, can lead to embolism in the water-conducting cells. The details and mechanisms of embolism repair in vascular plants are still not well understood. In particular, experimental results which indicate that embolism repair may occur during xylem tension cause great problems with respect to current paradigms of plant water transport. The present paper deals with a theoretical analysis of interfacial effects at the pits (pores in the conduit walls), because it was suggested that gas–water interfaces at the pit pores may be involved in the repair process by hydraulically isolating the embolized conduit. The temporal behaviour of bubbles at the pit pores was especially studied since the question of whether these pit bubbles are able to persist is of crucial importance for the suggested mechanism to work. The results indicate that (1) the physical preconditions which are necessary for the suggested mechanism appear to be satisfied, (2) pit bubbles can achieve temporal stability and therefore persist and (3) dissolving of bubbles in the conduit lumen may lead to the final breakdown of the hydraulic isolation. The whole process is, however, complex and strongly dependent on the detailed anatomy of the pit and the contact angle.

1. Introduction

According to the cohesion-tension theory, upward water flow in land plants is generated by a pressure gradient originating in the water loss of transpiring leaves (Zimmermann, 1983; Tyree and Ewers, 1991). This mechanism may cause large tension gradients in the xylem, the water-conducting tissue of vascular plants although the magnitude of the tension is still under debate (Pickard, 1981; Holbrook et al., 1995; Pockman et al., 1995; Steudle, 2001). This paper will concentrate on an important aspect of xylem tension: the development of gas bubbles within the xylem conduits, the tracheids or vessels, which lead to blockage of water transport (Tyree and Sperry, 1989; Tyree and Yang, 1990; Milburn, 1991).

It is generally assumed that an embolism develops from an initially small, air filled cavity in the xylem. Numerous pores (pits), which represent gaps in the secondary cell wall, exist on the walls of tracheids or vessels. A porous membrane, the pit membrane, is located in the centre of the pits. According to the "air seeding hypothesis", air is drawn through the pores of the pit membrane into a functioning conduit and leads to embolism which prevents further water transport inside the now embolized conduit (Sperry and Tyree, 1988).

The xylem is able to recover from embolism (Tyree et al., 1999; Holbrook et al., 2001). It is assumed that one important factor is represented by the (positive) root pressure which removes the gas filled spaces within the conduits by forcing the bubbles into solution, because the xylem pressure has to exceed a certain threshold value for bubble dissolution, depending on the radius of the conduits (Tyree et al., 1999). A corresponding physical model is based on the pressure values and the geometry of the conduits (Yang and Tyree, 1992). Embolism recovery occurs, in fact, frequently

*Corresponding author. Institute for Geosciences, University of Tuebingen, Sigwartstrasse 10, Tuebingen 72076, Germany. Tel.: +49-7071-2973061; fax: +49-7071-295217.

E-mail address: anita.roth@uni-tuebingen.de (A. Roth-Nebelsick).

over night or during rain periods when pressure values inside the xylem favour bubble solution (Magnani and Borghetti, 1995). In vines, embolism recovery is observed during spring when high root pressures occur (Ewers et al., 1991; Cochard et al., 1994). Stem pressure can also be involved in embolism reversal (Sperry et al., 1988).

There is recent evidence that embolism represents a frequent and regular phenomenon during daily xylem water transport and can be removed (i) very quickly (within minutes) and (ii) possibly under xylem tension, that is, during transpiration (Salleo et al., 1996; McCully, 1999; Tyree et al., 1999). Experimental indications that embolism repair may occur under xylem tension represent a serious problem within the current paradigms of water transport. The various single questions arising through this observation are: (i) how does water move into an embolized conduit when negative pressures exist in the adjacent functioning conduits and (ii) how can under these circumstances pressure values be achieved in the embolized conduit which allow for bubble dissolution? Recently, it was suggested that (i) living cells within the xylem would be able to supply embolized conduits with water, and (ii) surface properties and pit geometry of the conduits cause special interfacial effects which lead to hydraulic isolation and contribute to bubble dissolution (Holbrook and Zwieniecki, 1999).

Anatomical studies carried out by Zwieniecki and Holbrook (2000) corroborate this suggestion, because contact angle and pit geometry are in agreement with the physical pre-conditions of this model. However, no further physical analysis of this putative mechanism, which relies heavily on thermodynamic processes, exists so far. The temporal course of bubble growth or bubble dissolution is especially of crucial importance to embolism repair. The present paper concentrates on a detailed physical analysis of the interfacial processes which can take place if bubbles appear in xylem conduits. This analysis includes the temporal behaviour of bubbles in the lumen of xylem conduits, interfacial effects which can be expected at the pit and how these effects influence pressure within "pit bubbles" and their temporal dynamics. The analysis starts with the consideration of a simple spherical bubble and the results will be integrated into the exploration of which requirements are necessary for a successful "valve" function of a bubble situated at a pit pore.

2. Dynamics of a spherically symmetric bubble

2.1. Volume, surface tension, pressure and number of gas molecules of a spherically symmetric bubble

In the following sections, it will be described how the temporal behaviour of a gas bubble immersed in a liquid

can be derived from parameters such as bubble volume, pressure inside and outside the bubble, surface tension, temperature and dissolution dynamics of the gas molecules inside the bubble. We consider a spherically symmetric gas bubble of radius R. Its volume (cf. Fig. 1) is

$$V = \frac{4\pi}{3} R^3. \tag{1}$$

The pressure p inside the bubble (cf. Fig. 2) is given by the Young–Laplace equation as the sum of the pressure p_s in the surrounding liquid and a second term which stems from the surface tension γ of the gas/liquid interface,

$$p = p_s + \frac{2\gamma}{R}. \tag{2}$$

By treating the gaseous content of the bubble as an ideal gas, we can calculate the number n of gas molecules inside
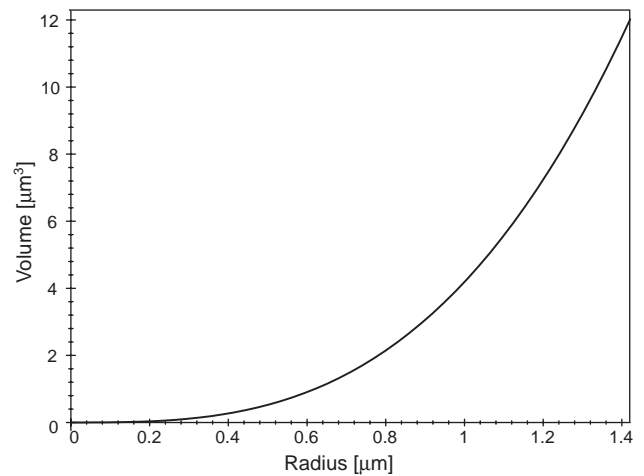

Fig. 1. Bubble volume V as a function of bubble radius R, according to Eq. (1) (cases 1–4, see text).
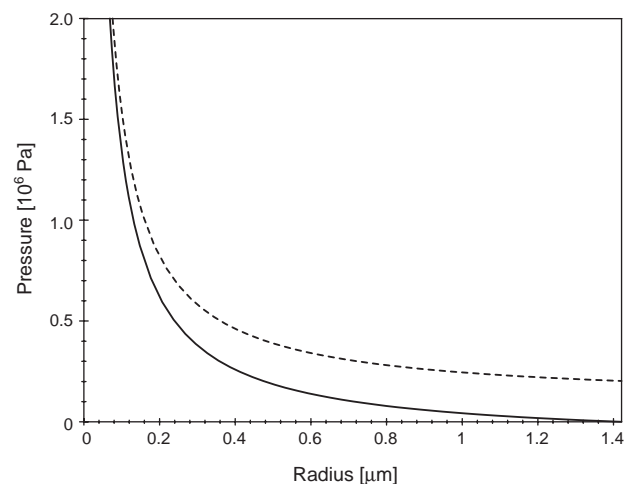

Fig. 2. Pressure p in the bubble as a function of bubble radius R, according to Eq. (2). The pressure p_s in the surrounding liquid amounts to $p_s = 101\,325$ Pa (broken line, cases 1 and 2) and $p_s = -101\,325$ Pa (solid line, cases 3 and 4), respectively (see text). Surface tension of water: $\gamma = 0.072$ N/m.
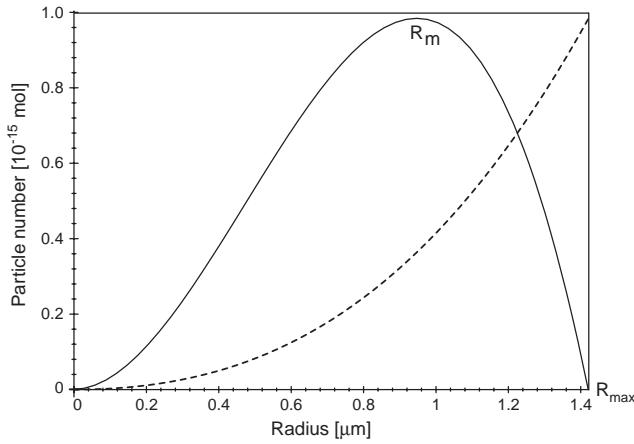
Fig. 3. Particle number n in the bubble as a function of bubble radius R, according to Eq. (3). The pressures p_s in the surrounding liquid have values $p_s = 101\,325$ Pa (broken line, cases 1 and 2) and $p_s = -101\,325$ Pa (solid line, cases 3 and 4), respectively. Absolute temperature: $T = 298$ K, gas constant: $\mathscr{R} = 8.314$ m³Pa/mol/ K.

the bubble from the equation for a perfect gas (note that $\mathscr{R}$ represents the gas constant and not a radius, T denotes absolute temperature, cf. Fig. 3):

$$n = \frac{pV}{\mathscr{R}T} = \frac{1}{\mathscr{R}T}\frac{4\pi}{3}(p_s R^3 + 2\gamma R^2). \qquad (3)$$

Before inspecting Eq. (3) further, we notice that the surface tension γ is always positive, whereas the pressure p_s in the liquid is not, because negative pressures can occur in the xylem. The cases $p_s > 0$ and $p_s < 0$ lead to quite different behaviour, as will become evident in the following sections.

Eq. (3) shows that $n(R)$ becomes zero at $R = 0$, whatever value p_s attains. We first consider the case of $p_s > 0$. This means for the plant that no xylem tension exists. This is the case, for example, during the night or in periods of rainfall and high humidity. A positive xylem pressure implies that $n(R)$ is a positive and monotonically increasing function of R for $R \geqslant 0$. No bubble (and therefore no gas particles) exist for $R = 0$, but for $R > 0$ an expanding bubble can house increasing numbers of gas particles. This behaviour is illustrated by Fig. 3. According to Eq. (2), the pressure p inside the bubble then approaches the pressure p_s of the surrounding liquid asymptotically with increasing bubble radius. Now we consider the case $p_s < 0$. Negative xylem pressure (i.e. xylem tension) can occur in the xylem during transpiration and/or water stress. For $p_s < 0$, the function $n(R)$ has a second zero on the positive R-axis at

$$R_{max} := \frac{2\gamma}{-p_s}. \qquad (4)$$

This is depicted by Fig. 3. In the case of $p_s < 0$, the function $n(R)$ is thus positive only if R lies in the interval $0 \leqslant R \leqslant -2\gamma/p_s$. Since $n(R)$ is a continuous function, it

must attain an extremum for some R-value within this interval, which lies at

$$R_m := -\frac{4\gamma}{3p_s}. \qquad (5)$$

Insertion of Eq. (5) into Eq. (3) returns that the maximum number of gas molecules, which can be accomodated in a spherically symmetric bubble surrounded by a liquid at negative pressure, depends only on the temperature T, the gas constant $\mathscr{R}$, the pressure $p_s < 0$ (the negative xylem pressure) and the surface tension γ of the gas/liquid interface. The maximum number of gas molecules is given by

$$n_{max} := \frac{2\pi\gamma}{\mathscr{R}T}\left(\frac{8\gamma}{9p_s}\right)^2. \qquad (6)$$

The existence of this maximum can be understood in terms of physics. The gas molecules with their inherent tendency to expand the volume that they occupy, are "kept together" by (i) the surface tension and (ii) the pressure p_s of the surrounding liquid as long as the latter quantity is positive. A negative liquid pressure p_s, however, acts "in the same direction" as the (potentially) expanding gas particles and the confinement of the gas molecules must be provided solely by the surface tension term in Eq. (2). Since the volume and the surface of a sphere are proportional to R^3 and R^2, respectively, and the former grows more rapidly with R than the latter, it is intuitively evident that the surface tension will be dominated by the volume pressure beyond a certain R-value. Consequently, the number of particles which can be accomodated within the bubble without risk of bursting is limited.

We summarize at the end of this section that under negative xylem pressure:

(i) a gas bubble can only contain a certain maximum number of gas molecules and
(ii) the radius of a gas bubble has an upper limit.

2.2. Physical basis of temporal bubble behaviour

We now proceed to the dynamics of the bubble. Our goal is to calculate $R(t)$, i.e. the temporal behaviour of the radius of the bubble. Once $R(t)$ is known, the functions $V(t)$, $p(t)$ and $n(t)$ can be derived from relations (1), (2) and (3).

For the sake of simplicity, we assume that the gas particles inside the bubble and the external liquid belong to different chemical species, i.e. air inside the bubble and water outside. This simplification limits our model to embolism events caused by "air seeding". This is a reasonable limitation, resting on two arguments: (i) There is evidence that most embolism events are caused by "air seeding" (Sperry et al., 1996), (ii) although water

molecules tend to vaporize into bubbles consisting initially only of air, their fraction of the total particle content will usually remain small, because it is proportional to the ratio between the water vapour pressure and the total pressure in the bubble. Thus, if the latter amounts to $p = 1$ atm $= 101\,325$ Pa, at a temperature of 25°C only about 3.2% of the particles in the bubble are water molecules. Under this assumption the dynamic behaviour of the bubble rests upon two physical effects:

(i) when gas contacts a liquid at an interface, gas particles dissolve into the liquid according to Henry's Law which states that the (partial) pressure of the gas (inside the bubble) p and the concentration C_R of the dissolved gas particles in the liquid in the near vicinity of the bubble (which is the meaning of the index R) are proportional to each other (see Fig. 4):

$$C_R = k_H p, \tag{7}$$

(ii) if the concentration of dissolved gas particles in the surrounding liquid deviates from the value C_R, diffusional currents, directed from areas of higher to areas of lower concentration arise.

As the combined result of both processes we expect that gas particles are transported either out of and away from the gas bubble or into the opposite direction. This process continues until an equilibrium situation is attained.
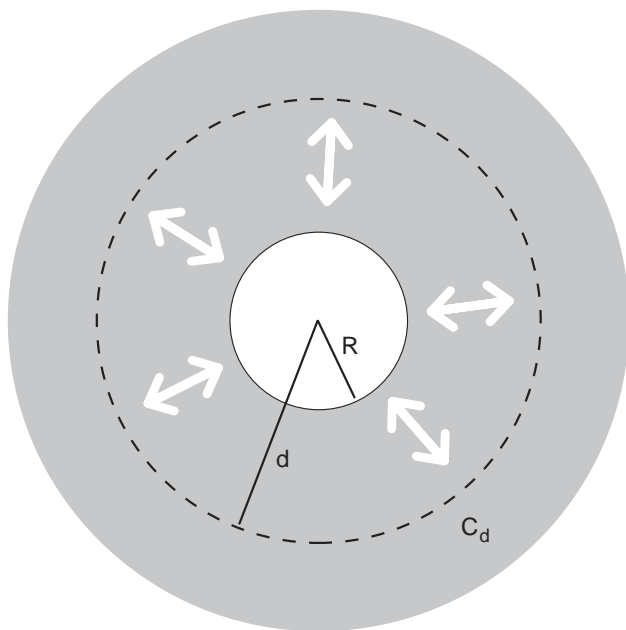
2.3. Calculation of temporal evolution of spherically symmetric bubbles

Our starting point to calculate $R(t)$ is the observation, that changes in the number n of gas particles in the bubble must be generated by the diffusional current I, as long as no other processes take place which consume (or produce) gas particles. The corresponding equation reads as

$$-\frac{dn}{dt} = I. \tag{8}$$

Since we adopt the convention that a positive diffusional current transports particles *away* from the bubble, Eq. (8) contains a minus sign. By means of the chain rule of differentiation we conclude

$$-\frac{dn}{dt} = -\frac{dn}{dR}\frac{dR}{dt} = I, \tag{9}$$

which implies the equation

$$\frac{dt}{dR} = -\frac{dn/dR}{I}. \tag{10}$$

$n(R)$ is already explicitly given in Eq. (3). If the current I can also be written as a function of R, the R-dependence of the right-hand side of Eq. (10) can be calculated and the integration

$$t(R) = -\int \frac{dn/dR}{I(R)}\, dR \tag{11}$$

can be performed. The calculation of $I(R)$ is provided in the Section A.1. Fig. 5 illustrates the results concerning

Fig. 4. Schematic representation of a gas bubble (white) of radius R immersed in a liquid (grey). Outside of a sphere of radius d (broken line) the air concentration in the liquid is held at a constant value C_d. In general, this gives rise to a radial diffusional current (white arrows).
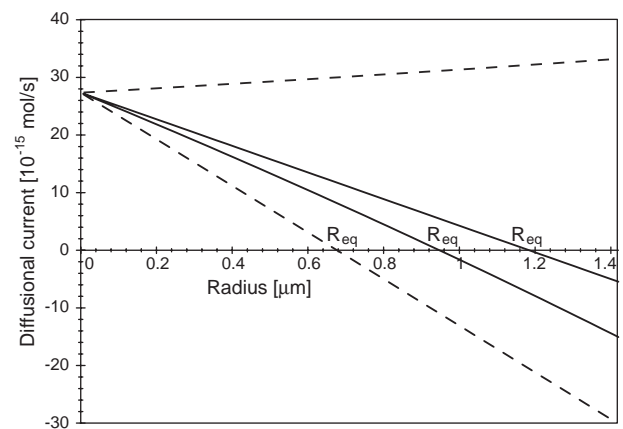

Fig. 5. Diffusional currents directed into or out of the bubble as a function of bubble radius. The four curves correspond to cases 1–4 (see text). The equilibrium radius R_{eq} is defined in Eq. (17) and characterizes the bubble radius where diffusion ceases. The pressure p_s in the surrounding liquid and the pressure p_d (equivalent to the air concentrations C_d at a radial distance $d = 15\,\mu$m from the bubble) have the following values: $p_s = 101\,325$ Pa, $p_d = 91\,193$ Pa (case 1, upper broken line) $p_s = 101\,325$ Pa, $p_d = 253\,313$ Pa (case 2, lower broken line) $p_s = -101\,325$ Pa, $p_d = 20\,265$ Pa (case 3, lower solid line) and $p_s = -101\,325$ Pa, $p_d = 11\,458$ Pa (case 4, upper solid line), respectively. Effective diffusion coefficient of air in water: $S = 1.95 \times 10^{-9}$ m^2/s, Henry's Law constant: $k_H = 7.75 \times 10^{-6}$ mol/m^3/Pa.

$I(R)$ for four different cases (explained in the following sections). Insertion of Eqs. (A.9) and (A.10) (from Appendix A) into Eq. (11) and subsequent integration leads to

$$t(R) = \alpha(R - R_0) + \beta(R^2 - R_0^2) + \delta(R^3 - R_0^3)$$
$$+ \; \varepsilon \log\left(\frac{R - R_{eq}}{R_0 - R_{eq}}\right). \tag{12}$$

R_0, the constant of integration in Eq. (12), is defined by $t(R_0) = 0$. Thus, R_0 denotes the bubble radius at time $t = 0$. The greek letters in Eq. (12) represent combinations of the constants $\mathscr{R}$, γ, S and k_H and the parameters T, R_{eq}, R_m and d.

$$\alpha := \frac{2}{3\mathscr{R}TSdk_H}\frac{R_{eq}}{R_m}(d - R_{eq})(R_m - R_{eq}), \tag{13}$$

$$\beta := \frac{-1}{3\mathscr{R}TSdk_H}\frac{R_{eq}}{R_m}(R_m - R_{eq} + d), \tag{14}$$

$$\delta := \frac{2}{9\mathscr{R}TSdk_H}\frac{R_{eq}}{R_m}, \tag{15}$$

$$\varepsilon := \frac{2}{3\mathscr{R}TSdk_H}\frac{R_{eq}^2}{R_m}(d - R_{eq})(R_m - R_{eq}), \tag{16}$$

with R_{eq} as the "equilibrium radius" ($R = R_{eq}$ implies $I = 0$, as is shown in Section A.2)

$$R_{eq} := \frac{2\gamma k_H}{C_d - k_H p_s} = \frac{2\gamma}{p_d - p_s}. \tag{17}$$

The pressure $p_d := C_d/k_H$ has been introduced in the last expression purely for mathematical convenience. (Physically, it can be interpreted as the partial pressure of (gaseous) air which is in equilibrium with (liquid) xylem sap containing air molecules in a concentration C_d.) The "equilibrium radius" R_{eq} defined in Eq. (17) represents the "final" radius of a bubble in those cases, in which diffusion ceases after some time. A closer inspection of Eqs. (12) and (A.11) (of Appendix A) reveals that four qualitatively different cases of bubble behaviour exist:

Case 1 : $0 < p_d < p_s$,
Case 2 : $0 < p_s < p_d$,
Case 3 : $p_s < -2p_d < 0$,
Case 4 : $-2p_d < p_s < 0$. \hfill (18)

Eq. (12) gives the time t as a function of the bubble radius R. This may appear to be strange at first sight, but as Eq. (12) is built up from a polynomial in R and a logarithmic term containing R, R cannot be expressed as a function of t. For the problem of exploring the temporal development of a bubble it is completely irrelevant whether the radius or the time is the independent variable.

The temporal behaviour of the bubbles for the four different cases is illustrated in Figs. 6, 7, 8 and 9. A short discussion of the different cases will be provided in the following sections.
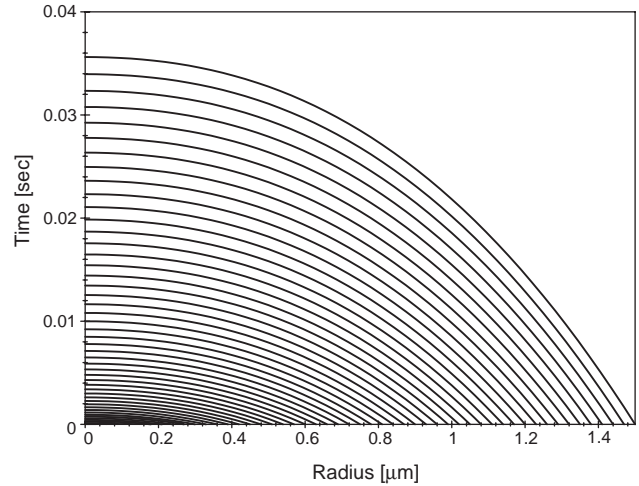

Fig. 6. Temporal development of a spherically symmetric gas bubble which is coupled by diffusion to a gas reservoir at constant pressure. The bubble radius R is drawn along the abscissa, time t along the ordinate. Each curve starts for $t = 0$ at an initial radius R_0. In case 1, the present case, every curve either terminates at $R = 0$ (because the corresponding bubble has dissolved) or it extends till infinity. Figures were obtained from Eq. (12) by insertion of the following parameter values $d = 15\,\mu m$, $p_e = 101\,325$ Pa, $p_d = 91\,193$ Pa (case 1).
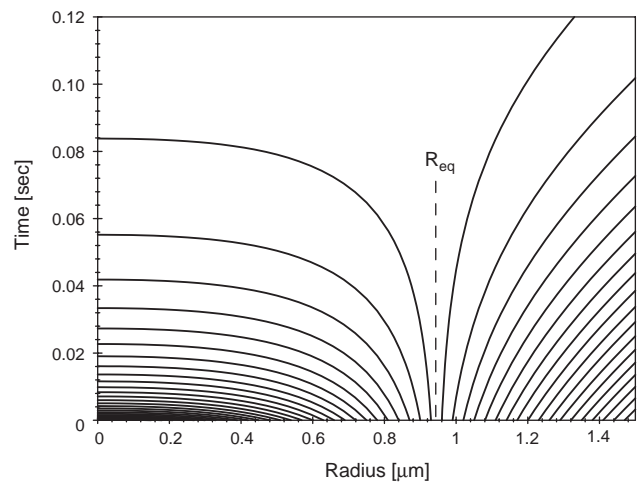

Fig. 7. Temporal development of a spherically symmetric gas bubble which is coupled by diffusion to a gas reservoir at constant pressure. The bubble radius R is drawn along the abscissa, time t along the ordinate. Each curve starts for $t = 0$ at an initial radius R_0. In case 2, the present case, every curve either terminates at $R = 0$ (for values of R_0 small enough), or it extends till infinity (because the corresponding bubble expands forever). R_{eq} denotes the bubble radius where diffusion ceases (for detailed explanation see text). Figure was obtained from Eq. (12) by insertion of the following parameter values $d = 15\,\mu m$, $P_e = 101\,325$ Pa, $P_d = 253\,313$ Pa (case 2).
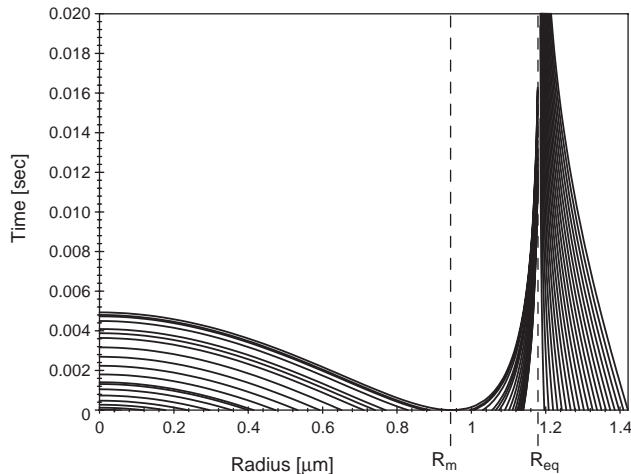
Fig. 8. Temporal development of a spherically symmetric gas bubble which is coupled by diffusion to a gas reservoir at constant pressure. The bubble radius R is drawn along the abscissa, time t along the ordinate. Each curve starts for $t = 0$ at an initial radius R_0. In case 3, the present case, every curves either terminates at $R = 0$ (for value of R_0 small enough), or it extends till infinity (because the corresponding bubble stops its expansion, if the diffusional current ceases). R_m denotes the radius at which the capacity of the bubble to host particles is at its maximum. R_{eq} denotes the bubble radius where diffusion ceases (for detailed explanation see text). Figure was obtained from Eq. (12) by insertion of the following parameter values $d = 15$ μm, $P_e = -101\,325$ Pa, $P_d = 20\,265$ Pa (case 3).
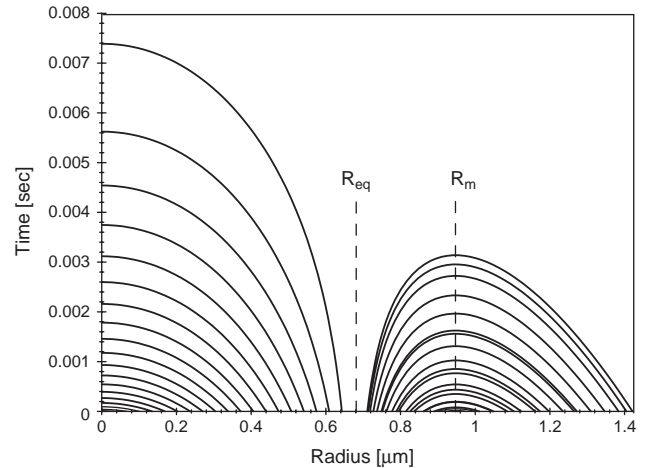

Fig. 9. Temporal development of a spherically symmetric gas bubble which is coupled by diffusion to a gas reservoir at constant pressure. The bubble radius R is drawn along the abscissa, time t along the ordinate. Each curve starts for $t = 0$ at an initial radius R_0. The curves with $R > R_{eq}$ is case 4, the present case, are physically impossible and will be discussed in the Appendix A. R_m denotes the radius at which the capacity of the bubble to host particles is at its maximum. R_{eq} denotes the bubble radius where diffusion ceases (for detailed explanation see text). Figures were obtained from Eq. (12) by insertion of the following parameter values $d = 15$ μm, $P_e = -101\,325$ Pa, $P_d = 111\,458$ Pa (case 4).

2.4. Discussion of temporal evolution of spherically symmetric gas bubbles

Case 1 (*see Fig.* 6): For a positive pressure $0 < p < p_s$ of the liquid surrounding the gas bubble, the bubble will disappear after some time. According to the Young–Laplace equation and Henry's Law, the concentration of dissolved gas particles in the liquid in the near vicinity of the bubble is greater than their concentration at $r = d$. Hence, the diffusional current $I > 0$ is directed out of the bubble (see Fig. 5 or Eq. (A.9)). By losing gas molecules, the radius of the bubble decreases (see Fig. 3 or Eq. (3)), and the pressure inside increases (see Fig. 2 or Eq. (2)), which results in an ongoing efflux of particles of the bubble until it has dissolved. The "dissolution time" can either be taken from Figs. 6 and 7 (as the intersection of any curve starting at $R_0 < R_{eq}$ and the t-axis) or it can be calculated by setting $R = 0$ in Eq. (12). This case is realized in the xylem if, for example, small bubbles dissolve during the night or/ and under root pressure.

Case 2 (*see Fig.* 7): For $R_0 < R_{eq}$ the $t(R)$-curves show the same features as in case 1.

A bubble of the initial radius $R_0 > R_{eq}$, however, will not dissolve but grow (in principle indefinitely). $R_0 > R_{eq}$ implies that the concentration of the dissolved gas particles adjacent to the bubble is smaller than their concentration at $r = d$. Thus, the diffusional current $I < 0$ is directed into the bubble (Fig. 5), the particle

number $n(R)$ in the bubble increases and—according to Fig. 3—also its radius. This leads to a decreasing bubble pressure (Fig. 2) and to a diffusional current $I < 0$. This case represents conduit bubbles which cannot be dissolved due to, for example, inability of the plant to produce significant root pressure or large conduits which allowed for the development of correspondingly large bubbles (for example, after pit membrane damage by fatigue, Hacke et al., 2001). The large vessels of ring-porous woods are usually irreversibly blocked by embolism events and new functioning vessels are formed in the following growing season.

Case 3 (*see Fig.* 8): The (R, t)-plot (Fig. 8) shows a more complex structure than in the preceding cases. For $R < R_m$ the interpretation is equal to case 1. This means that bubbles with an initial radius smaller than R_m dissolve despite $p_s < 0$. For $R_m < R < R_{eq}$, the diffusional current $I > 0$ is directed out of the bubble (Fig. 5). However, due to the existence of the maximum $n_{max} = n(R_m)$, the loss of particles leads to an increase in R (Fig. 3). This leads to a decrease of p (Fig. 2) and a subsequent decrease of $I > 0$. The process of particle loss slows down as R approaches R_{eq} asymptotically and stops eventually—in theory after an infinite, in reality after a finite amount of time.

A similar behaviour develops for $R > R_{eq}$. Since $I < 0$ is directed into the bubble (Fig. 5), n increases and R decreases (Fig. 3). This leads to an increase in p (Fig. 2), which slows down the particle influx via $I < 0$. Again, R

approaches R_{eq} and the whole process stops in an "asymptotic" manner at $R = R_{eq}$. We may say, that the equilibrium at $R = R_{eq}$ is stable in case 3, because after a small perturbation of the bubble radius (say, to a new radius $R = R_{eq} + \rho$ with $|\rho| \ll R$) the equilibrium at $R = R_{eq}$ will restore. A formal derivation of this statement will be provided in Section A.3.

Case 4 (*see Fig.* 9): For $R < R_{eq}$ the interpretation is as in case 1, that is, the bubble will dissolve after a certain time interval.

If $R > R_{eq}$ in Fig. 9, the bubble appears to show an "impossible" behaviour: time appears to "stop" at $R = R_m$ for all curves who start at a $R_0 > R_{eq}$. In all other cases, the (R, t)-curves behave as expected: they extend either to temporal infinity (at $R = R_{eq}$ or for $R \to \infty$) or they intersect after a finite "dissolution time" with the t-axis, because the bubbles have shrunk to the radius $R = 0$, i.e. they have completely dissolved. The strange behaviour of bubbles with $R_0 > R_{eq}$ shown in Fig. 9 can be traced to the fact that for this special case the equations presented in this paper have been stressed beyond their "physical limit". This will be discussed in the following.

From Figs. 5 and 3 we see that for every $R > R_{eq}$ the diffusional current is directed into the bubble and that this influx of particles makes the bubble radius approach $R = R_m$, which represents the radius with the maximum of n. At $R = R_m$ the current $I < 0$ still transports particles into the bubble, although it cannot accomodate additional particles. The strange behaviour of the (R, t)-curves in Fig. 9 is an attempt of our mathematical framework to deal with this contradiction although the validity of Eq. (8) (which states that the bubbles's only way to lose particles is by means of a diffusional flux out of the bubble) is already exhausted at $R = R_m$.

What happens in reality is that the bubble deals with the breakdown of Eq. (8) by splitting up into "daughter bubbles". This behaviour is certainly beyond the limits of Eq. (8). Once the daughter bubbles have formed, they *do* again obey Eq. (8), until they reach the radius $R = R_m$ (which may or may not happen) and the splitting event repeats.

It is impossible to predict the number, sizes and respective particle contents of the daughter bubbles within the framework of the actual equations. Still, we may be confident that the gross number of all particles within all bubbles present is the same before and after a splitting event. Eq. (3) connects the number of particles in a bubble n with its radius R. Viewed as an equation for R, Eq. (3) has two real solutions (that is, if R_m is positive, a negative R_m implies one real solution). Thus, even if the number of particles within a bubble "born" in a splitting event would be known in advance, the ambiguity with respect to its radius would remain.

We now provide a short summary of this section. Four different cases of bubble evolution arise, depend-ing on xylem pressure and air concentration in the xylem sap. Under positive xylem pressure, the bubble can dissolve or it can grow (cases 1 and 2). Under negative xylem pressure, bubbles with sufficiently small initial radii dissolve (cases 3 and 4), the bubbles can grow asymptotically until an equilibrium radius $R = R_{eq}$ is reached (case 3), or splitting of the bubbles can occur (case 4). The temporal development of a bubble with $R > R_{eq}$ in case 4 can be characterized as a succession of time intervals with predictable behaviour, punctuated by events with unpredictable outcome. It is possible to calculate from Eq. (8) (or, rather from its solution, Eq. (12)), when the next bubble splitting event will occur. It is, however, not possible to calculate when the event following the next one will take place. Since we do not really need this information for our present considerations, it suffices to keep in mind, that whenever in case 4 the bubble radius attains the value $R = R_m$, our central vehicle of prediction (i.e. Eq. (8)) is superseded by a process, whose outcome is only partially predict-able. The temporal course of splitting events is further discussed in Section A.2.

3. Dynamics of an axially symmetric pit bubble

3.1. Background and basics of repair scenario

The model of Holbrook and Zwieniecki (1999) and Zwieniecki and Holbrook (2000) comprises the follow-ing components (see Fig. 10):

(i) The positive pressure in the embolized conduit (in contrast to the negative pressures within the functioning conduits) promotes the dissolution of the gas bubble.
(ii) The process of dissolution is enhanced by the surface tension of the liquid/gas interface which adds to the pressure of the liquid.
(iii) If the resulting pressure in the gas bubble is sufficiently high, a diffusional flux of dissolved air molecules to the adjacent conduits develops.
(iv) The pits connecting embolized and functioning conduits show a special geometry. Their shape leads to hydraulic isolation of the embolized vessel from the adjacent conduits, because the effect of surface tension of the liquid/gas interface and the pressure of the liquid diminish each other. There-fore, dissolution of the bubbles at/within the pits (termed as "pit bubbles", PB, throughout the rest of the paper) is less effective if compared to the dissolution of the bubbles within the conduit lumen (termed as "lumen bubbles", LB, throughout the rest of the paper). In fact the pressure difference between them may cause a diffusional current which "feeds" the PB at expense of the LB.
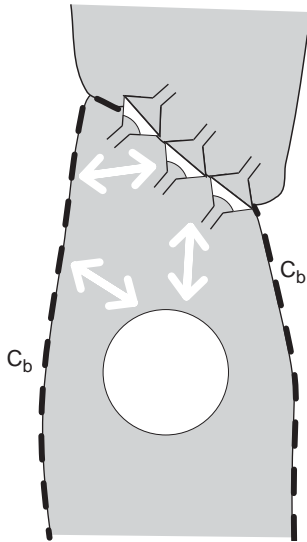
Fig. 10. Schematic representation of an embolized vessel (lower part of figure) filled with xylem sap under positive pressure p_e and an intact vessel (upper part of figures) filled with liquid under tension (negative pressure). White: gas. White arrows symbolize diffusional currents between the LB, the PBs and the adjacent conduits. The broken line along the border of the vessel indicates a constant air concentration C_b in the xylem sap of the adjacent conduits. This figure depicts the realistic situation.
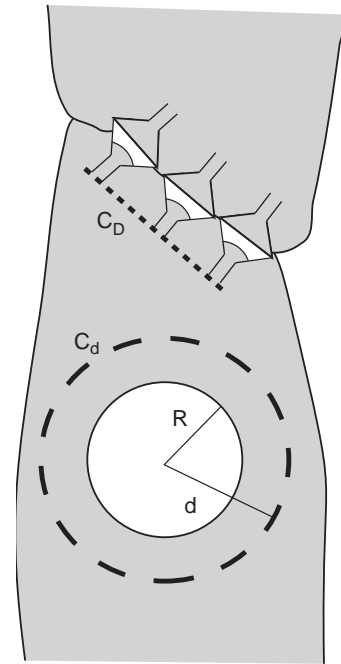

Fig. 11. Schematic representation of an embolized vessel (lower part of figure) filled with xylem sap under positive pressure p_e and an intact vessel (upper part of figure) filled with liquid under tension (negative pressure). White: gas. The broken lines labelled c_d and c_D denote the reservoirs of constant air concentration to which the PBs and the LB, respectively, are coupled by diffusion. This figure depicts the approximate treatment of the situation.

The success of this model depends largely on the question if the dissolution of the "embolizing bubbles" can be completed before the hydraulic isolation of the embolized vessel fails due to the dissolution of the PB. Therefore, the temporal behaviour of both spherically symmetric LB and of axially symmetric PB is of central significance to embolism repair and to the general dynamics of bubbles in xylem conduits.

Since an exact mathematical description of the situation is impossible and a near-exact treatment requires extensive use of numerical mathematics (which is beyond the scope of this contribution), we pursue an approximate quantitative approach to the processes which are happening after an air seeding event.

In reality (see Fig. 10) LB and PB interact, because generally the pressures in the LB and in the PB are not the same and they are both different from the pressure C_b/k_H, equivalent to the air concentration C_b in the adjacent conduits. Therefore, diffusional currents be-tween all three develop, which couple the dynamics of the LB and the PB. Fig. 11 indicates the approximations we employ (i) to break up this coupling on the mathematical level and (ii) to obtain simple boundary conditions on simply shaped geometrical forms, exhibit-ing a high degree of symmetry. We assume that the LB exchanges particles only with a sphere of radius d around the LB where the air concentration in the liquid has the constant value C_d. Similarly, the row of PB is supposed to have diffusional contact only to a "bar" at

a distance D from the pit necks. Thus, the constant air concentration C_b of the adjacent conduits has been replaced by the constant air concentration C_d which is also present in the embolized vessel, with the exception of the sphere of radius d around the LB. In a sense, the constant air concentration C_D at distance D from the pit necks replaces the diffusional current between the LB and the PB. The dynamics of the LB and the PB are no longer coupled.

The following part of the paper concentrates on the putative "valve" function of PB. Hereby, the results of the analysis of LB dynamics are used as basis for the far more complex problem of the interfacial effects at the PB. We discuss the dynamics of a PB under the aspect of achieving the hydraulic isolation of an embolized vessel from its intact neighbours. Thus, we assume that the liquid in the embolized vessel is under a positive pressure $p_e > 0$ while in its intact neighbour conduit (on the other side of the pit) a negative pressure $p_i < 0$ remains.

3.2. Compatibility conditions between pit geometry and pressure difference across the interface

A gas/liquid interface within a cone-shaped pit may be realized according to Holbrook and Zwieniecki (1999) and Zwieniecki and Holbrook (2000) as in

Fig. 12: the area between the gas/liquid interface (in the embolized side of the pit) and the membrane is filled with gas and the interface bulges towards the pit membrane.

An interface is capable to maintain hydraulic isolation of an embolized vessel only if the pit geometry and the pressures concerned fulfil several conditions (see Fig. 12):

(i) the gas/liquid interface should bulge towards the pit membrane,
(ii) the gas/liquid interface should not touch the pit membrane, because then hydraulic isolation of the embolized vessel would break down,
(iii) if the gas/liquid interface is situated at the mouth of the pit neck, it should not retreat further,
(iv) the pressure in the gaseous part of the pit should be positive, because we assume it to be filled with an ideal gas and ideal gases do not exhibit attractive forces between their constituents,
(v) the interface should be able to provide the required pressure difference.

In order to formulate these conditions in mathematical terms we characterize the position of the interface by the variable l (i.e. the distance between interface and membrane, measured along the "side" of the pit as in Fig. 12). Trigonometric relations allow then the expression of R in terms of the contact angle θ, the parameters s and α (characterizing the shape of the pit) and the variable l:

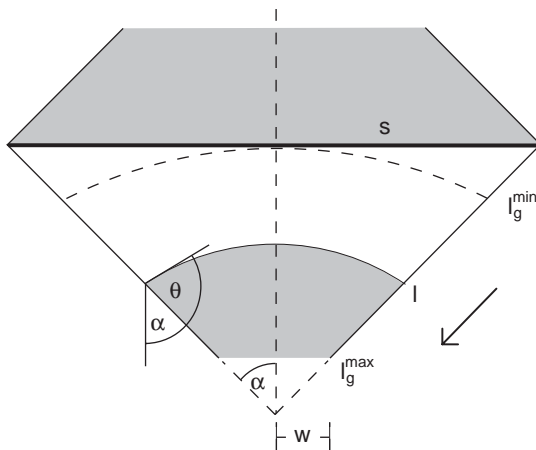$$R = \frac{s - l\sin\alpha}{-\cos(\alpha + \theta)}. \tag{19}$$

Fig. 12. Schematic representation of a pit, isolating an intact (upper part of figure) from an embolized vessel (lower part of figure). The quantity l characterizes the position of the gas/liquid interface, $l = 0 =$ position of the membrane.

white: air, grey: water, s: radius of pit membrane, θ: contact angle, α: pit opening half-angle, w: radius of pit neck, l_g^{min}: minimum value of l due to condition (22), l_g^{max}: maximum value of l due to condition (23).

θ and α are restricted by definition and geometry, respectively, to the intervals (see also Fig. 12):

$$0 \leqslant \theta \leqslant \pi \quad \text{and} \quad 0 \leqslant \alpha \leqslant \frac{\pi}{2}. \tag{20}$$

The conditions now read as

(i) $$\theta + \alpha > \frac{\pi}{2}. \tag{21}$$

If condition (21) is fulfilled, R is positive: Eq. (20) implies $\pi/2 < \alpha + \theta \leqslant 3\pi/2$. The cosine is negative on this interval.

(ii) Assuming that the membrane remains flat under all circumstances (which cannot be taken for granted, because the membrane must necessarily sustain the high pressure difference between the intact vessel and the gaseous interior of the pit, see Fig. 12), geometric relations (consult Fig. 12) imply the following conclusion:

$$l \geqslant s\frac{1 - \sin(\alpha + \theta)}{\sin\alpha - \cos\theta} =: l_g^{min}. \tag{22}$$

(iii) Denoting the radius of the pit neck by w, Fig. 12 implies

$$l \leqslant \frac{1}{\sin\alpha}(s - w) =: l_g^{max}. \tag{23}$$

(iv) Denoting the pressures in the intact and embolized vessels by $p_i < 0$ and $p_e > 0$, respectively, the Young–Laplace equation takes the form:

$$p = p_e - \frac{2\gamma}{R} = p_e + 2\gamma\frac{\cos(\alpha + \theta)}{s - l\sin\alpha}. \tag{24}$$

Recalling that the pressure is positive in the embolized vessel ($p_e > 0$) and negative in the intact one ($p_i < 0$), Eq. (24) implies that values of the expression $2\gamma/R$ which are too large result in a negative pressure in the gas bubble within the pit. The condition

$$p \geqslant 0 \tag{25}$$

transforms upon use of Eq. (24) into a geometric condition on l:

$$l \leqslant \frac{1}{\sin\alpha}\left(s + \frac{2\gamma}{p_e}\cos(\alpha + \theta)\right) =: l_p^{max}. \tag{26}$$

(v) The maximum pressure difference Δp^{max} which can, in principle, be sustained by the interface (while bulging into the required direction and obeying condition (21), ignoring, however, restriction (26)), is identical to the maximum of the expression $2\gamma/R$. This lies at $l = l_g^{max}$ (i.e. at the mouth of the pit neck), because $2\gamma/R$ increases for increasing values of l, as is evident from Eqs. (19)

and (20). Thus,

$$\Delta p^{max} = \frac{2\gamma}{R}\bigg|_{l=l_g^{max}} = -\frac{2\gamma\cos(\alpha+\theta)}{w}. \tag{27}$$

As the pressure p in the gaseous part of the pit cannot drop below $p = 0$, a sufficient condition to be met by the gas/liquid interface is given by the relation

$$\Delta p^{max} \geqslant p_e, \tag{28}$$

which can be obtained formally by insertion of Eq. (27) into Eq. (24) and setting $p = 0$.

Results (ii)–(v) summarize to the following relations ($\min(x,y)$ denotes the smaller of x and y):

$$l_g^{min} \leqslant l \leqslant \min(l_g^{max}, l_p^{max}) \quad \text{and} \quad \Delta p^{max} \geqslant p_e. \tag{29}$$

Eqs. (29) can be read as compatibility conditions between the quantities defining the pit and the pressure p_e: an interface can only be realized, if the conditions

$$l_g^{min} \leqslant \min(l_g^{max}, l_p^{max}) \quad \text{and} \quad \Delta p^{max} \geqslant p_e \tag{30}$$

are satisfied.

Since Eqs. (28), (27), (19) and the definition of l_g^{max} (Eq. (23)) lead to the statements ($\Delta p^{max} \geqslant p_e \Rightarrow l_g^{max} \geqslant l_p^{max}$) and ($\Delta p^{max} \geqslant p_e \Rightarrow \min(l_g^{max}, l_p^{max}) = l_p^{max}$), conditions (30) for the existence of an interface can be rephrased in the form

$$\Delta p^{max} \geqslant p_e \quad \text{and} \quad l_g^{min} \leqslant l_p^{max}. \tag{31}$$

Employing the definitions of the quantities Δp^{max}, l_g^{min} and l_p^{max}, conditions (31) can be cast into the form

$$\frac{2\gamma}{s}\frac{\sin\alpha - \cos\theta}{\cos\alpha} \leqslant p_e \leqslant \frac{2\gamma}{w}(-\cos(\alpha+\theta)) \tag{32}$$

which is especially well suited to enquire into the effects of changes in the pit defining quantities s, w and α or in the contact angle θ on the acceptable range of p_e.

3.2.1. Comparison with measurements

Values of the maximum pressure differences reported in the literature amount to $p_e \approx 150\,000$ Pa. The magnitude of values concerning the contact angle θ and the pit opening half-angle α appear to amount roughly to $\theta \approx 50°$ and $\alpha \approx 75°$, respectively, and the radii of the pit membrane and the pit neck are given as $s \approx 2.5$ μm and $w \approx 0.5$ μm (Zwieniecki and Holbrook, 2000; van Ieperen et al., 2001). The maximum pressure difference and the boundaries of the l-interval resulting from these values are found from Eqs. (27), (22), (23) and (26): $\Delta p^{max} = 165\,190$ Pa, $l_g^{min} = 1.39$ μm, $l_g^{max} = 2.07$ μm, $l_p^{max} = 2.02$ μm. Application of conditions (30) yields the following result:

$$l_g^{min} = 1.392 \text{ μm} < 2.02 \text{ μm} = l_p^{max} = \min(l_g^{max}, l_p^{max}), \tag{33}$$

$$\Delta p^{max} = 165\,190 \text{ Pa} \geqslant 150\,000 \text{ Pa} \approx p_e, \tag{34}$$

that is, with the pit data given above, all conditions are met and we can proceed to the analysis of the PB dynamics.

3.3. Volume, surface tension, pressure and number of gas molecules of a pit bubble

We shall explore the dynamics of a PB with the same framework applied to the LB (Section 2).

The volume of a PB is obtained from Fig. 12 by adding and subtracting cones and sections of a sphere as (see also Fig. 13)

$$V = \begin{cases} \frac{\pi}{3}l^2\left(\frac{\cos\alpha}{-\cos(\alpha+\theta)}\right)\{3s\sin\theta - l[2\sin\alpha\sin\theta \\ \quad + \cos\alpha\cos\theta]\} \quad \text{if } 0 \leqslant l \leqslant l_g^{min}, \\ \frac{\pi}{3}s^3\cot\alpha \\ \quad -\frac{\pi}{3}\left(\frac{s-l\sin\alpha}{-\cos(\alpha+\theta)}\right)^3\{\cot\alpha[-\cos(\alpha+\theta)]^3 + \\ \quad [1-\sin(\alpha+\theta)]^2[2+\sin(\alpha+\theta)]\} \quad \text{if } l \geqslant l_g^{min}. \end{cases} \tag{35}$$

Eq. (35) is more complex than its counterpart, Eq. (1). The simplicity of the latter is due to: (i) the spherical symmetry of the LB (a sphere is completely described by its radius, for the still axisymmetric geometry of a pit, however, the three variables s, w and α are required), and (ii) the fact, that in the case of a spherically symmetric bubble the radius of curvature of its surface coincides with the radius of the bubble.
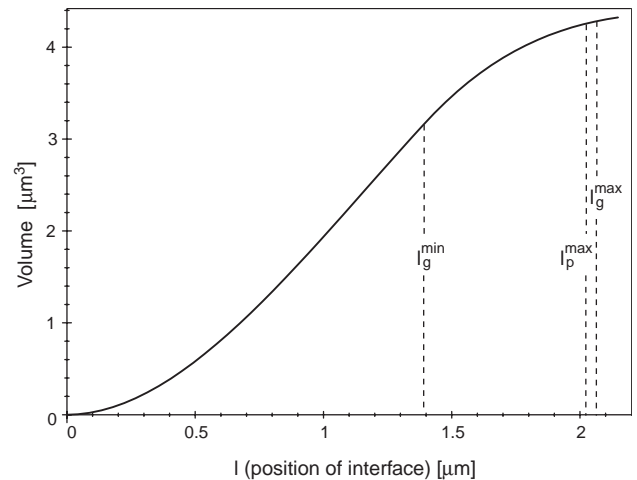

Fig. 13. Bubble volume V as a function of parameter l, according to Eq. (35) (cases A and B, see text). l (position of the air/water interface) is restricted to the interval $l_g^{min} < l < \min(l_p^{max}, l_g^{max})$ (for definitions see text). $\theta = 50°$, $\alpha = 75°$, $s = 2.5$ μm, $w = 0.5$ μm.

The pressure p inside the PB (cf. Fig. 14) is given by the Young–Laplace equation as

$$p = p_e - \frac{2\gamma}{R} = p_e - 2\gamma\left(\frac{-\cos(\alpha+\theta)}{s - l\sin\alpha}\right). \tag{36}$$

Eq. (36) is similar to Eq. (2) (provided the variable p_s in Eq. (2) attains negative values) in that the right-hand sides of both equations become zero for some value of R (respectively l) and the dynamics which develops is quite similar in both cases.

The number n of gas molecules inside the bubble follows from the equation for a perfect gas (cf. Fig. 15),

$$n = \frac{pV}{\mathcal{R}T} \tag{37}$$

with p and V as provided by Eqs. (35) and (36). A closer inspection of Eq. (37) would reveal that $n(l)$ has two zeros and a maximum within the interval $0 \leqslant l \leqslant s/\sin\alpha$. The zeros are inherited from the functions $V(l)$ and $p(l)$. The maximum follows because (i) the left zero derives from $V(l)$ and the right one from $p(l)$, (ii) $V(l)$ and $p(l)$
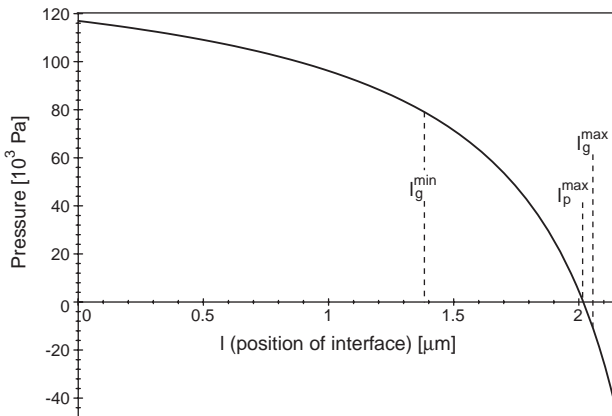

Fig. 14. Pressure p in the PB as a function of l, according to Eq. (36). The pressure p_e in the surrounding liquid amounts to $p_e = 150\,000$ Pa (cases A and B, see text).
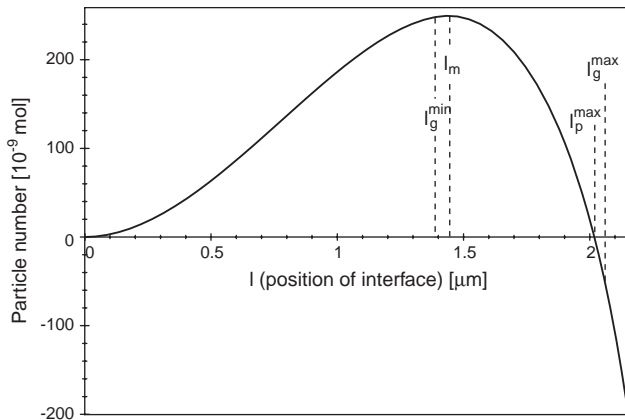

Fig. 15. Particle number n in the bubble as a function of l, according to Eq. (37). The pressure in the surrounding liquid has the value $p_e = 150\,000$ Pa (cases A and B, see text). Absolute temperature $T = 298$ K.

are continuous functions of l, and, (iii) $dV/dl \geqslant 0$ and $dp/dl \leqslant 0$ for $0 \leqslant l \leqslant s/\sin\alpha$. As dn/dl is a polynomial of fourth degree in l, attempts to calculate the position l_m of n_{max} on the l-axis lead to uncomfortably long expressions. Therefore, we restrict the treatment to define l_m by the equation $n(l_m) = n_{max}$ and to illustrate the situation by Fig. 15.

The principle result of this section is that a PB can—similarly as a LB under negative liquid pressure—contain only a certain maximum number of gas molecules without bursting immediately.

3.4. Dynamics of a cone-shaped pit

Our goal is to calculate $l(t)$. As before, we assume that changes in the number n of gas particles in the bubble are exclusively due to the diffusional current I:

$$-\frac{dn}{dt} = I. \tag{38}$$

This can be reformulated as

$$-\frac{dn}{dt} = -\frac{dn}{dl}\frac{dl}{dt} = I, \tag{39}$$

from which we conclude

$$\frac{dt}{dl} = -\frac{dn/dl}{I} \tag{40}$$

and

$$t(l) = -\int \frac{dn/dl}{I(l)}\,dl, \tag{41}$$

provided the diffusional current $I(l)$ is known. $I(l)$ is calculated in Section A.4 as Eq. (A.28) and depicted by Fig. 16. $n(l)$ is already provided by (37), insertion of
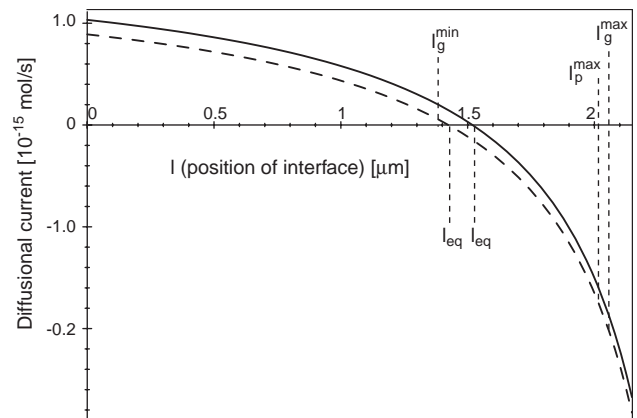

Fig. 16. Diffusional current directed into or out of the pit as a function of interface position l. The two curves correspond to cases A (broken line) and B (solid line). The equilibrium position l_{eq} is defined in Eq. (43) and characterizes the position of the interface where diffusion ceases. The pressures p_e in the surrounding liquid and the pressure p_D (equivalent to the air concentrations C_D at a distance D from the pit) amount to $p_e = 150\,000$ Pa, $p_D = 70\,000$ Pa (case A, solid line) and $p_e = 150\,000$ Pa, $p_D = 76\,500$ Pa (case B, broken line), respectively. For the description of cases A and B, see text.

dn/dl (from Eq. (37)) and $I(l)$ into Eq. (40) shows that the integrand is a rational function in l, which consists of a polynomial of fifth degree in the numerator over a polynomial of third degree in the denominator. Subsequent integration leads to a transcendental function in l with the following structure:

$$t(l) = \frac{1}{\delta_1 l + \delta_0} \times \{[\xi_1 l + \xi_0]$$
$$\times \log(\lambda_1 l + \lambda_0) + [\Xi_1 l + \Xi_0] \log(\Lambda_1 l + \Lambda_0)$$
$$+ v_4 l^4 + v_3 l^3 + v_2 l^2 + v_1 l + v_0\}$$
$$- \frac{1}{\delta_1 l_0 + \delta_0} \times \{[\xi_1 l_0 + \xi_0]$$
$$\times \log(\lambda_1 l_0 + \lambda_0) + [\Xi_1 l_0 + \Xi_0] \log(\Lambda_1 l_0 + \Lambda_0)$$
$$+ v_4 l_0^4 + v_3 l_0^3 + v_2 l_0^2 + v_1 l_0 + v_0\}. \quad (42)$$

l_0, the constant of integration in Eq. (42), is defined by $t(l_0) = 0$. Thus, l_0 denotes the position of the interface at time $t = 0$. The greek letters in Eq. (42) represent lengthy combinations of the constants $\mathscr{R}$, γ, S and k_H and the parameters T, l_{eq}, l_m, α, θ, s, w, C_D and D. The

"equilibrium interface position" ($l = l_{eq}$ implies $I = 0$ and $p_D = C_D k_H$) is found to be

$$l_{eq} := \frac{1}{\sin \alpha}\left(s + \frac{2\gamma}{p_e - p_D}\cos(\alpha + \theta)\right). \quad (43)$$

Figs. 17 and 18 illustrate the two distinct cases of pit behaviour which are possible, according to Eq. (42). Which case is realized depends on the relation between l_{eq} and l_m (the value of the parameter l at maximum number of molecules in the PB):

Case A : $l_{eq} \geqslant l_m$,
Case B : $l_{eq} \leqslant l_m$. $\quad (44)$

Comparison with Figs. 8 and 9 shows, that the PB behaves in entire analogy with a spherical bubble immersed in a liquid under negative pressure. Since cases A and B correspond to cases 3 and 4, respectively, a discussion of cases A and B can be omitted. We merely mention, that in case B, PB with their interface positioned initially at an $l_0 > l_{eq}$ should be treated as
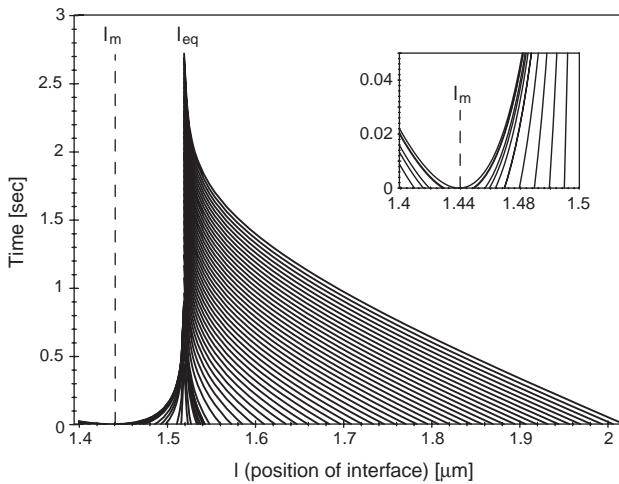

Fig. 17. Temporal development of an axisymmetric gas bubble in a pit which is coupled by diffusion to a gas reservoir at constant pressure. The insets show magnified details for small values of l and t. Time t is represented by the ordinate, the interface positions l by the abscissa. The abscissa terminates at the left at $l = l_g^{min}$ (for smaller l-values the interface would touch the pit membrane) and at the right at $l = l_p^{max}$ (greater l-values would lead to negative pressures within the gas bubble). l_m and l_{eq} denote the interface positions where the capacity of the bubble to host particles is at its maximum and where diffusion ceases, respectively. Each curve starts for $t = 0$ at an interface initial position l_0. Curves with $l_0 < l_m$ (see inset) describe PBs which dissolve, whereas curves starting at an $l_0 > l_m$ extend to temporal infinity, thus indicating that the interface approaches the equilibrium value $l = l_{eq}$. (case A, left). l_m and/or l_{eq} may be smaller than $l = l_g^{min}$ or greater than $l = l_p^{max}$. Their location depends on the values of p_e (pressure of the surrounding liquid) and p_D (pressure equivalent to the concentration $C_D = p_D k_H$ of gas particles in the surrounding liquid at a distance D from the pit). Since we want the figure to give a full picture of all effects possible, rather than to represent realistic cases, we have chosen $p_e = 150\,000$ Pa and $p_D = 70\,000$ Pa. Absolute temperature is $T = 298$ K. This case A illustrates.
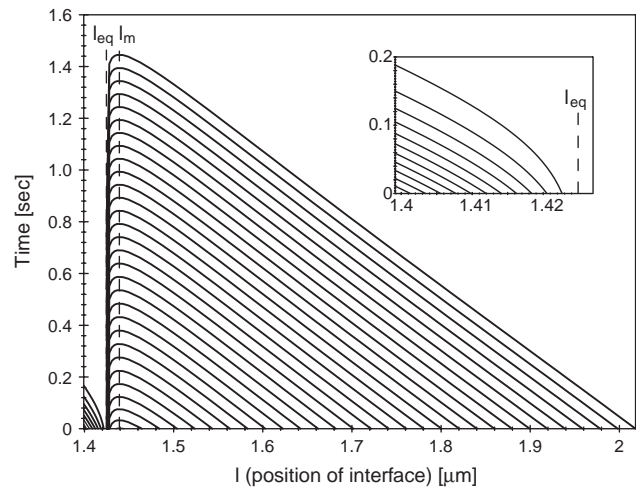

Fig. 18. Temporal development of an axisymmetric gas bubble in a pit which is coupled by diffusion to a gas reservoir at constant pressure. The insets show magnified details for small values of l and t. Time t is represented by the ordinate, the interface positions l by the abscissa. The abscissa terminates at the left at $l = l_g^{min}$ (for smaller l-values the interface would touch the pit membrane) and at the right at $l = l_p^{max}$ (greater l-values would lead to negative pressures within the gas bubble). l_m and l_{eq} denote the interface positions where the capacity of the bubble to host particles is at its maximum and where diffusion ceases, respectively. Each curve starts for $t = 0$ at an interface initial position l_0. PBs with their interface positioned initially at an $l_0 < l_{eq}$ (see inset) dissolve in the course of time while curves starting with an $l_0 > l_{eq}$ describe what happens if our system of equations exceeds its limits of competence. The problem can be resolved in the same way as in case 4 (Section 2 and Appendix A). l_m and/or l_{eq} may be smaller than $l = l_g^{min}$ or greater than $l = l_p^{max}$. Their location depends on the values of p_e (pressure of the surrounding liquid) and p_D (pressure equivalent to the concentration $C_D = p_D k_H$ of gas particles in the surrounding liquid at a distance D from the pit). Since we want the figure to give a full picture of all effects possible, rather than to represent realistic cases, we have chosen $p_e = 150\,000$ Pa and $p_D = 76\,500$ Pa (case B, right). Absolute temperature is $T = 298$ K. This depicts case B.

artefacts of our system of equations, rather than reality, in the same sense as their counterparts in case 4. A physically acceptable resolution of the problem with case B—the PB splits into daughter bubbles—follows the same principles as in case 4 (see also Section A.2).

The essential result of this section is that the PB can develop temporal stability (and only under this condition it can act as valve) if certain combinations of p_e and p_D exist in the conduit.

4. Bubble dynamics after air seeding events

4.1. Air seeding without embolism

An air seeding event does not necessarily embolize an intact vessel. If, according to Sections 2.1 and 2.3, the air sucked into the vessel develops into a (spherical) bubble which contains at most $n_{max} = (2\pi\gamma/\mathscr{R}T)(8\gamma/9p_s)^2$ particles, chances are good that the bubble behaves as described in cases 3 and 4: For $R_0 < R_m$ in case 3 and for $R_0 < R_{eq}$ in case 4 the bubble should have dissolved after some time.

For $R_0 > R_m$ in case 3, however, it should approach the equilibrium radius R_{eq}, and thus exist—in principle—indefinitely long. Within the framework of our equations (which quite naturally does not encompass all possible effects), a limited number of such non-expanding bubbles may be tolerated in an operating vessel. They can, however, disturb the metastable state of xylem tension and lead to its breakdown.

4.2. Repair after embolism

If, however, a bubble with $R_0 > R_{eq}$ develops according to case 4, or a bubble tries to form, which would contain $n > n_{max}$ particles, things are different: Then (in case 4, only when the radius $R = R_m$ has been reached) the expansion tendency of the gas particles due to their statistical movements inevitably outweighs the surface tension. Thus an equilibrium between the forces connected with both effects—which is a necessary condition for a bubble to establish itself—cannot be achieved. As discussed in Section A.2, the bubble will probably split up into daughter bubbles, which may or may not dissolve. The exact result of this situation is unpredictable, but it may well happen that repeated bursting of bubbles into daughter bubbles causes the water (which is in a metastable state under negative pressure) to "collapse" into a stable state. As a result, a positive water pressure establishes within the vessel and small gas bubbles drift into the pits connecting the embolizing vessel with its still intact neighbours. In the end, the ability of the vessel to conduct water has broken down completely.

According to the model of Holbrook and Zwieniecki (shortly described in Section 3.1) the repair scenario should now be initiated. In view of our results we reexamine three crucial aspects of the model, namely the questions (i) under which circumstances a diffusional flux of dissolved air molecules to the adjacent conduits establishes, (ii) whether the embolized vessel remains hydraulically isolated during the dissolution process, and (iii) how and when this hydraulic isolation breaks down.

(i) As the liquid pressure p_e is positive in an embolized vessel, it behaves according to cases 1 or 2 (notice, that when cases 1 and 2 are employed to describe a LB in an embolized vessel, p_s and p_e denote the same pressure). For $p_d < p_e$ case 1 is realized and the LB dissolves for all initial radii R_0 (see Fig. 6, notice that dissolution is not restricted to the R_0-values of the figure, e.g. a bubble with $R_0 = 50 \mu m$ needs under otherwise identical conditions about 20 s for dissolution). For $p_d > p_e$ case 2 (Fig. 7) is realized and the LB dissolves only if $R_0 < R_{eq}$ (which is in view of Eq. (17) equivalent to the condition $p_e < p_d < p_e + 2\gamma/R_0$), otherwise (for $p_d > p_e + 2\gamma/R_0$) it expands until it fills the lumen completely.

Since the concentration C_d of air dissolved in the xylem sap has in most cases presumably a value such that the condition $p_d < p_e$ is satisfied (recall that p_d is defined by $C_d = k_H p_d$), a LB will quite probably dissolve after some time, provided the embolized bubble remains hydraulically isolated during the dissolution process.

(ii) In terms of Figs. 17 and 18 an interface maintains hydraulic isolation (in principle) indefinitely long, if its (l, t)-curve approaches $l = l_{eq}$. Curves, which intersect the vertical line $l = l_g^{min}$ indicate hereby, that the interface touches the membrane and that hydraulic isolation fails due to bursting of the PB. If case A is realized, interfaces initially at a $l_0 < l_m$ do not isolate, those initially at a $l_0 > l_m$ do. Interfaces which behave according to case B are unsuited for isolation purposes, because they either (for $l_0 < l_{eq}$) move towards and touch eventually the membrane, or (for $l_0 > l_{eq}$) they run through a sequence of splitting events in the sense of Section A.2.

Consulting Fig. 19, we see that the relative positions of l_g^{min}, l_g^{max}, l_p^{max} and l_m depend on the pressure p_e. We furthermore observe, that for $p_e < p_e^{crit}$ (with $p_e^{crit} \approx 135\,000$ Pa for the values of the pit geometry and the contact angle chosen in Section 3) l_m is smaller than l_g^{min}. In view of Fig. 17, which illustrates case A, the inequality $p_e < p_e^{crit}$ implies that curves with $l_0 < l_m$ (leading to isolation failure) do not exist, that is, all interfaces approach
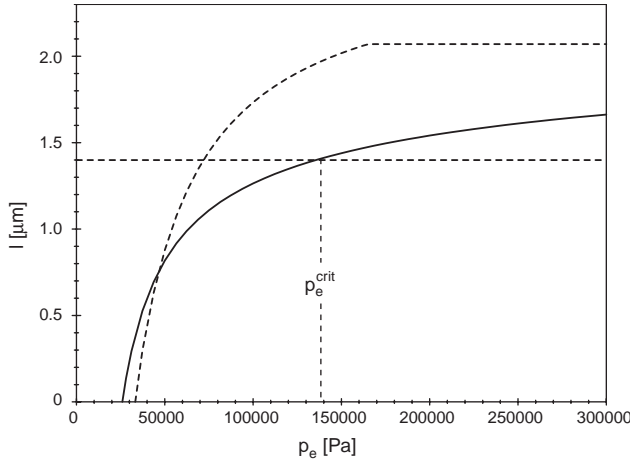
Fig. 19. $\min(l_g^{max}, l_p^{max})$ (curved broken line), l_g^{min} (straight broken line) and l_m (solid line) as functions of the pressure p_e in the xylem sap. $l_m(p_e)$ and l_g^{min} intersect at $p_e = p_e^{crit}$. The values of the pit geometry and the contact angle chosen in Section 3 imply $p_e^{crit} \approx 135\,000$ Pa.

l_{eq} (preserving isolation). Related to Fig. 18, which illustrates case B, condition $l_m < l_g^{min}$ (which is equivalent to $p_e < p_e^{crit}$) implies that all curves intersect the vertical line $l = l_g^{min}$, which means failure of isolation. Since case B is defined via the condition $l_{eq} < l_m$, we conclude: if the pit is exposed to the pressure $p_e < p_e^{crit}$, hydraulic isolation is preserved as long as the relation $l_{eq} > l_g^{min}$ is valid. When l_{eq} drops below l_g^{min}, isolation fails almost immediately (see Figs. 20–22).

This result is a general one, although we do not give explicitly p_e^{crit} as a function of the contact angle θ, the pit opening half-angle α and the radii s and w of pit membrane and pit neck, respectively. This is, because $p_e^{crit}(\theta, \alpha, s, w)$ is equivalent to and would have to be solved for from the equation $l_m = l_g^{min}$, which is possible in principle but beyond the scope of the present contribution.

We should point out that the values of the pressures p_e and p_D (or, rather, the "boundary concentration" $C_D = k_H p_D$ of air in water) leading to Figs. 17 and 18 were primarily chosen with respect to the purpose of illustrating all possible aspects of cases A and B. In an embolized vessel, a value of the pressure p_e of the xylem sap around 1 atm = 101 325 Pa appears to be not unreasonable, because it is the pressure of the atmosphere. Even if the plant is capable somehow to exert an additional pressure on the embolized vessel, the value $p_e^{crit} \approx 135\,000$ Pa leaves some margin for the relation $p_e < p_e^{crit}$ to be satisfied. Remember, however, that the value of $p_e^{crit}(\theta, \alpha, s, w)$ is species dependent.

(iii) Figs. 23 and 24 (and, more generally, Eq. (43) upon differentiation with respect to p_D) show that l_{eq} is a monotonically decreasing function of p_D. That is,
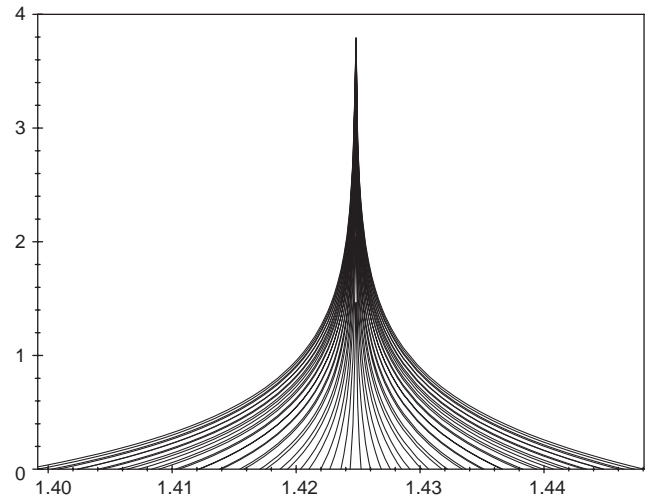

Fig. 20. Sequence of (t, l)-curves for the p_D-value 1500 Pa. Time $t(\Delta)$ is drawn along the ordinate, the interface position l (μm) along the abscissa. The pressure of the xylem sap is $p_e = 75\,000$ Pa. The sequence of Figs. 20–22 illustrate a section of the curve $l_{eq}(p_D)$ in Fig. 23. The parameter values in this figure satisfy $l_m < l_g^{min} < l_{eq}$. The present figure (and Fig. 21) describe pits which preserve hydraulic isolation (every interface approaches $l = l_{eq}$, reaches it after at most 3.5 s and stays there infinitely).
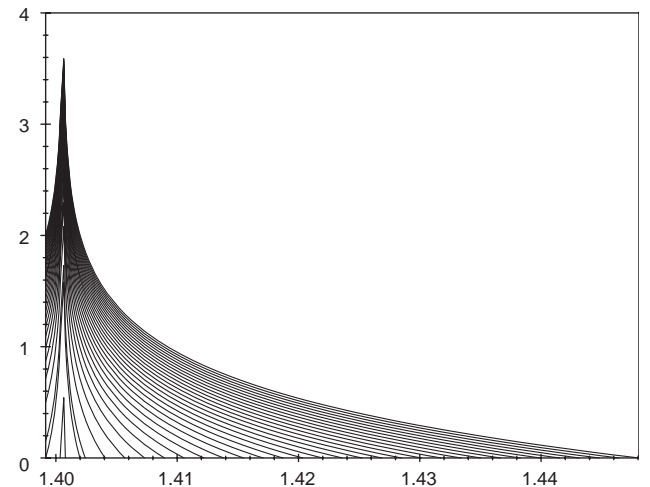

Fig. 21. Sequence of (t, l)-curves for the p_D-value 3000 Pa. Time t (s) is drawn along the ordinate, the interface positions l (μm) along the abscissa. The pressure of the xylem sap is $p_e = 75\,000$ Pa. The sequence of Figs. 20–22 illustrate a section of the curve $l_{eq}(p_D)$ in Fig. 23. The parameter values in this figure satisfy $l_m < l_g^{min} < l_{eq}$. Fig. 20 and the present figure (Fig. 21) describe pits which preserve hydraulic isolation (every interface approaches $l = l_{eq}$, reaches it after at most 3.5 s and stays there infinitely).

there are values of p_D which satisfy the inequality $l_{eq}(p_D) > l_g^{min}$ (implying that the respective interface maintains hydraulic isolation). If we increase p_D, the value of $l_{eq}(p_D)$ decreases and reaches eventually values $l_{eq}(p_D) < l_g^{min}$ (which indicate the loss
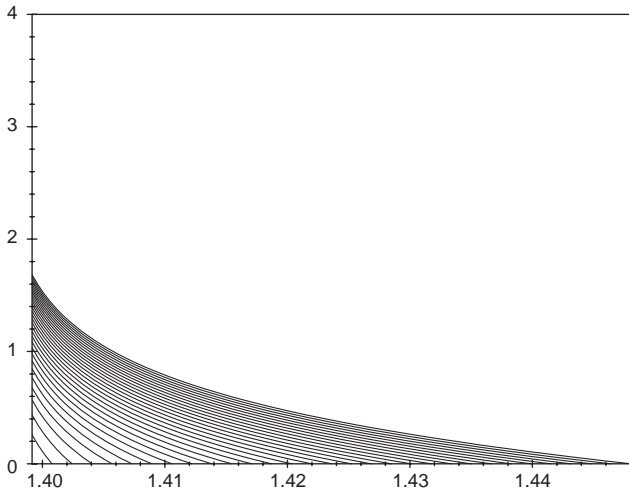
Fig. 22. Sequence of (t, l)-curves for the p_D-value 3250 Pa. Time t (s) is drawn along the ordinate, the interface positions l (μm) along the abscissa. The pressure of the xylem sap is $p_e = 75\,000$ Pa. The sequence of Figs. 20–22 illustrate a section of the curve $l_{eq}(p_D)$ in Fig. 23. The present figure is based upon the relation $l_m < l_{eq} < l_g^{min}$. The pits considered by this figure become permeable because every interface approaches the pit membrane and touches it after at most 1.7 s.
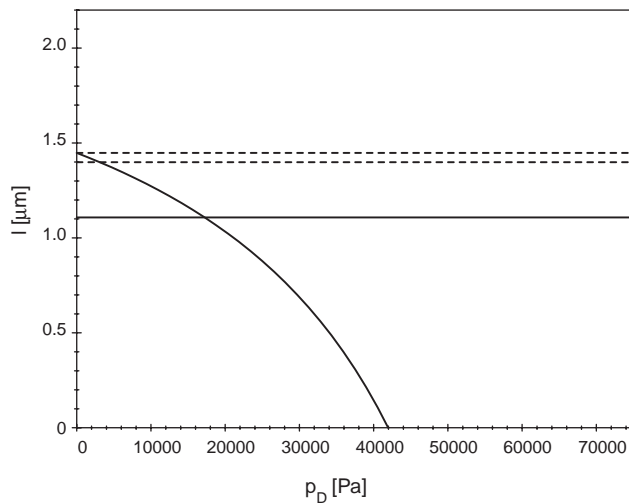

Fig. 23. $\min(l_g^{max}, l_p^{max})$ (upper broken line), l_g^{min} (lower broken line), l_m (solid line, horizontal) and l_{eq} (solid line, curved) as functions of the pressure p_D, which stands for the air concentration $C_D = k_H p_D$ in the xylem sap at a distance D from the pit neck (see Figs. 11 and 26). The gas/liquid interface in a pit provides hydraulic isolation, if (i) l_m lies below the lower broken line (i.e $l_m < l_g^{min}$), and (ii) $l_{eq}(p_D)$ lies between the broken lines (i.e. $l_g^{min} < l_{eq} < \min(l_g^{max}, l_p^{max})$). In the present figure, $p_e = 75\,000$ Pa, that is, $p_e < p_e^{crit}$. Thus, condition (i) is fulfilled and the gas/liquid interface in the PB behaves as in case A (see Fig. 17). Figs. 20–22 are related to Fig. 23, the present figure in that the former can be viewed as "realizations" of the latter for different values of the variable p_D. In Figs. 20 and 21 conditions (ii) is also fulfilled and hydraulic isolation thus realized, in Fig. 22 it is not.

of the isolation ability of the pit, as explained above).

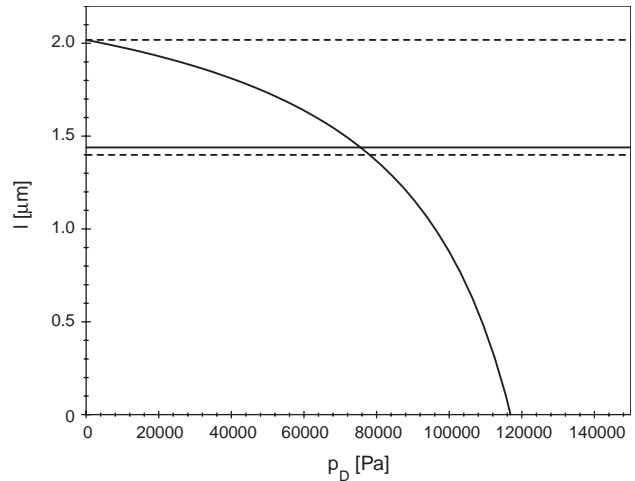Recalling from Fig. 2 (or from the Young–Laplace equation) that the pressure within a

Fig. 24. $\min(l_g^{max}, l_p^{max})$ (upper broken line), l_g^{min} (lower broken line), l_m (solid line, horizontal) and l_{eq} (solid line, curved) as functions of the pressure p_D, which stands for the air concentration $C_D = k_H p_D$ in the xylem sap at the distance D from the pit neck (see Figs. 11 and 26). The gas/liquid interface in a pit provides hydraulic isolation, if (i) l_m lies below the lower broken line (i.e. $l_m < l_g^{min}$), and (ii) $l_{eq}(p_D)$ lies between the broken lines (i.e. $l_g^{min} < l_{eq} < \min(l_g^{max}, l_p^{max})$). In the present figure, $p_e = 150\,000$ Pa, that is, $p_e > p_e^{crit}$. Thus, condition (i) is not fulfilled and the gas/liquid interface in the PB behaves as in case A (see Fig. 18). Hydraulic isolation cannot be achieved, although condition (ii) is fulfilled for a wide range of p_D-values. The values of the pit geometry and the contact angle chosen in Section 3 imply $p_e^{crit} \approx 135\,000$ Pa.

spherical bubble grows rapidly with decreasing bubble radius, Henry's Law implies an increasing air concentration in the liquid around the LB during the dissolution process, in fact, it culminates at the moment when the LB disappears.

We propose, that the combination of both effects cause the breakdown of hydraulic isolation as the last act of the repair process. We cannot become more specific at this point, because the mathematics we have used so far is too simple to express (or predict) the time of isolation breakdown as a function of pit geometry, vessel geometry, contact angle, of the pressures involved and of the number of particles trapped initially in an LB. The reason for the complexity of these processes is primarily due to the diffusional currents which evolve between the LB, the PB and the adjacent conduits (see Fig. 10). To describe the situation more accurately, the diffusion equation must be solved in at least two dimensions and more sophisticated approximations for the boundary conditions must be employed.

5. Final conclusions

This first physical analysis provides evidence that (i) the preconditions for the mechanism are satisfied

(within the chosen parameters), (ii) temporally stable PB can establish and that (iii) the breakdown of the pit bubbles can be initiated by the final stage of the repair process. The results summarized so far thus indicate that the mechanism suggested by Holbrook and Zwieniecki (1999) is principally able to cause hydraulic isolation of an embolized conduit. The results, however, also show that the underlying physical processes are very complex and depend heavily on the geometric properties of the pits, on the developing contact angle and on the gas concentration in the sap. Further analyses of the bubble behaviour in xylem conduits are expected to yield a more detailed understanding of the involved mechanisms and of the role of interfacial effects. Since the considered processes cannot be observed directly, theoretical analyses of this subject are an indispensable tool for improving our knowledge of the significance of interfacial effects for plant water transport.

Appendix A

A.1. Diffusion equation and diffusion current $I(R)$ in a spherically symmetric situation

For the sake of simplicity, we assume the following (see Fig. 4): (i) The gas bubble is surrounded by an (imaginary) sphere-shaped closed surface with radius d which resides completely within the vessel lumen. This sphere serves as source or sink for the diffusing gas particles. (ii) Outside of this closed surface the concentration of dissolved gas particles is kept constant at the value C_d. Thus, we restrict the process of diffusion to a spherical section of the vessel lumen which contains the gas bubble, and we assume that the air concentration in the xylem sap exterior to this section remains constant. Due to this auxiliary construction the whole system is spherically symmetric and can conveniently be parametrized with the radial coordinate r, the distance to the centre of the bubble.

In order to calculate $I(R)$ we first have to solve the diffusion equation for the area between $r = R$ and d.

The time-independent diffusion equation for spherical symmetry reads as

$$\frac{1}{r^2}\frac{d}{dr}\left(r^2\frac{dC}{dr}\right) = 0. \tag{A.1}$$

The general solution of this equation contains two arbitrary constants, a and b,

$$C(r) = a + \frac{b}{r}. \tag{A.2}$$

The solution $C(r)$ is subject to the boundary conditions

$$C(R) = C_R \quad \text{and} \quad C(d) = C_d. \tag{A.3}$$

C_R means the concentration of air in the near vicinity of the bubble and C_d denotes the (constant) concentration

of air in the liquid, the xylem sap (as depicted in Fig. 4). Application of the boundary conditions (A.3) results in

$$C(r) = \frac{C_d d - C_R R}{d - R} + \frac{Rd}{d - R}(C_R - C_d)\frac{1}{r}. \tag{A.4}$$

The current density $\vec{j}$ of the gas particles diffusing through the liquid follows from (A.4) according to Fick's Law

$$\vec{j} = -S\, grad\, C, \tag{A.5}$$

where S represents the effective conductance of the liquid for the diffusing substance. Due to spherical symmetry only the radial component of $\vec{j}$ remains,

$$j(r) = -S\frac{dC(r)}{dr} = S\frac{Rd}{d - R}(C_R - C_d)\frac{1}{r^2}. \tag{A.6}$$

The (total) current I including all gas particles diffusing into or out of the gas bubble is given by integration over the (closed) surface of a sphere centered at $r = 0$ with a radius r_a which may lie anywhere in the interval $R < r_a < d$:

$$I = \oint \vec{j} \cdot d\vec{A} = j(r_a)r_a^2 \int_0^\pi \sin\theta\, d\theta \int_0^{2\pi} d\phi$$
$$= 4\pi j(r_a)r_a^2 = 4\pi S\frac{Rd}{d - R}(C_R - C_d). \tag{A.7}$$

Eq. (A.7) states that the gas bubble is in equilibrium with the environment (i.e. no gas particles are exchanged), when there is no diffusion current. How C_R is dependant on R follows from Henry's Law (7) and the Young–Laplace equation (2),

$$C_R = k_H p_s + \frac{2\gamma k_H}{R}. \tag{A.8}$$

This one-to-one relation between C_R and R is the basis of the geometric characterization of the equilibrium situation $C_R = C_d$ (equivalent to $I = 0$ by (A.7)) via the "equilibrium radius" $R_{eq} = 2\gamma/(p_d - p_s)$ of definition (17): Substitution of $R = R_{eq}$ in (A.8) leads to $C_R = C_d$ and hence to $I = 0$.

Eventually, after insertion of Eqs. (A.8) and (17) we obtain the explicit R-dependence of Eq. (A.7)

$$I(R) = 8\pi S\gamma k_H \frac{d}{R_{eq}}\frac{R_{eq} - R}{d - R}. \tag{A.9}$$

For the evaluation of the integral in Eq. (11) we need a second ingredient beneath $I(R)$. Using Eq. (5) in order to eliminate p_s in favour of R_m from dn/dR we obtain

$$\frac{dn}{dR} = \frac{16\pi\gamma}{3\mathscr{R}T}\frac{R}{R_m}(R_m - R). \tag{A.10}$$

We note that the interpretations of the quantities R_m and R_{eq} are significant only if the relations $p_s < 0$ and $p_d - p_s > 0$, respectively, are valid, i.e. if the xylem pressure is negative. Eqs. (5) and (17), however, can and will be viewed as formal definitions of R_m and R_{eq} also for positive xylem pressure, in the sense of a shorthand

notation. Interpretations in terms of radii are, however, not valid then.

By using Eqs. (A.9) and (A.10) we obtain from Eq. (10)

$$\frac{dt}{dR} = \frac{-2}{3\mathscr{R}TSdk_H}(d-R)R\frac{R_{eq}}{R_m}\frac{R_m - R}{R_{eq} - R}, \qquad (A.11)$$

the desired integrand of Eq. (11).

A.2. Detailed discussion of a lumen bubble (LB) according to case 4

Fig. 25 gives a more realistic picture of the temporal development of a case 4-bubble than Fig. 9. The upper part of the figure shows the number of particles $n(R)$ in the bubble, its lower part represents typical examples on a bubble's (R, t)-path (the path given here describes the fate of just one bubble, the sister or daughter bubbles do not appear). The (R, t)-path consists of two types of curves:

- the curves $0 \to 1-$, $1+ \to 2-$, $2+ \to 3-$, $2' + \to 3'$, and beyond $3+$ represent time segments, which are predicted by Eq. (8),
- the straight lines $1- \to 1+$, $2- \to 2+$, $2- \to 2'+$ and $3- \to 3+$ stand for the "jumps" in radius R caused by the formation of daughter bubbles whenever the bubble radius R takes on the value $R = R_m$.

The quantities Δn_1, Δn_2, $\Delta n_{2'}$ and Δn_3 in the upper part of the figure are related to the numbers of particles lost from the considered bubble during the splitting events $1- \to 1+$, $2- \to 2+$, $2- \to 2'+$ and $3- \to 3+$.

The bubble's route through the (R, t)-plain evolves as follows:

- Starting at a radius $R = R_0$ (point 0) the bubble develops according to Eq. (8) until it undergoes a non-predictable splitting event at $1-$. Then it loses Δn_1 particles, which forces its radius to jump to one of the two solutions of Eq. (3) for $n = n_{max} - \Delta n_1$. We suppose that the value R_{1+} is realized.
- Curve $1+ \to 2-$ again obeys Eq. (8), at $2-$ the bubble experiences a second splitting, the particle loss amounts to Δn_2. Again, the bubble radius may jump to either of the two R-values R_{2+} or $R_{2'+}$.
- If the bubble happens to "choose" the latter value, the diffusional current, which has procured particles so far, is from now on directed out of the bubble, and the bubbles fate is, according to Eq. (8), to evaporate particles until its existence ceases at $3'$.
- If the bubble radius takes on the latter value, the diffusional current is again directed into the bubble, the curve $2+ \to 3-$ evolves according to Eq. (8), a third splitting of the bubble occurs at $3-$, combined with a particle loss Δn_3, and so on.
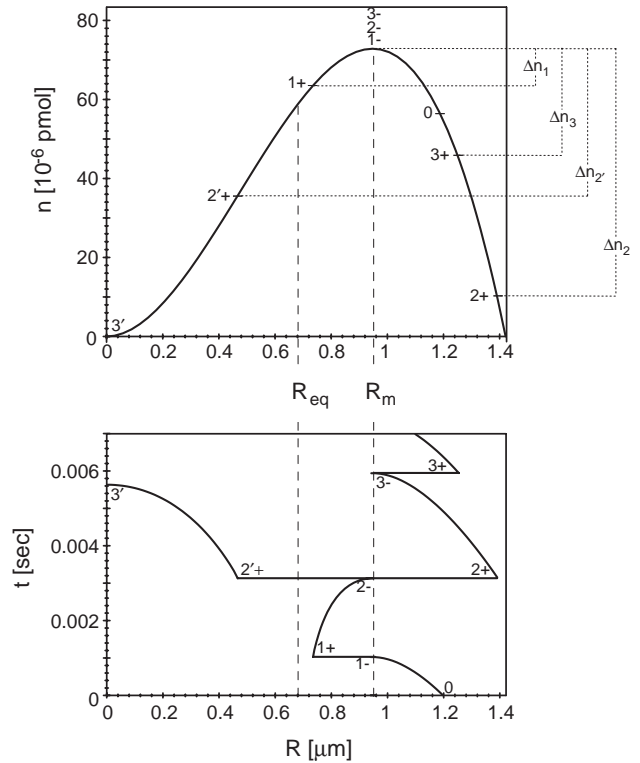

Fig. 25. Upper part: Particle number $n(R)$ as a function of bubble radius R of a gas bubble in a liquid (case 4, i.e. $0 < R_{eq} < R_m$, equivalent to $0 < -p_s < p_d$). Lower part: Possible (t, R)-path of a gas bubble in case 4 (for explanation see text).

A.3. Stability of the diffusional equilibrium at $R = R_{eq}$

In order to shed some light onto the nature of the equilibrium characterized by $I = 0$, or, in geometric terms, by $R = R_{eq}$, we examine the system's behaviour if it is initially in equilibrium (i.e. no diffusional current) and then slightly perturbed. In order to define this we expand Eq. (8) about $R = R_{eq}$ after setting $R(t) = R_{eq} + \rho(t)$. Since we assume $|\rho| \ll R$ it is sufficient to keep only the linear terms in ρ. The expansions

$$n(R) \approx n(R_{eq}) + n'(R_{eq}) \cdot \rho, \qquad (A.12)$$

$$I(R) \approx I(R_{eq}) + I'(R_{eq}) \cdot \rho \qquad (A.13)$$

(a prime stands for differentiation with respect to R) reduce upon differentiation with respect to t (which is characterized by a dot) and in view of the condition of equilibrium $I(R_{eq}) = 0$ to

$$\dot{n}(R) \approx n'(R_{eq}) \cdot \dot{\rho}, \qquad (A.14)$$

$$I(R) \approx I'(R_{eq}) \cdot \rho. \qquad (A.15)$$

Insertion into Eq. (8) and reorganization leads to the linear first order differential equation

$$\dot{\rho} + \frac{I'(R_{eq})}{n'(R_{eq})}\rho = 0 \qquad (A.16)$$

with the readily obtained solution

$$\rho(t) = \rho_0 \exp\left(-\frac{I'(R_{eq})}{n'(R_{eq})}t\right). \tag{A.17}$$

ρ_0, the constant of integration, characterizes the radial distance by which the bubble has been disturbed initially, at $t = 0$.

The interpretation of the result (A.17) is straightforward: An initial perturbation ρ_0 "dies out" with an characteristic "decay time" $\tau := n'(R_{eq})/I'(R_{eq})$ if the expression

$$\frac{n'(R_{eq})}{I'(R_{eq})} = \frac{2}{3\mathcal{R}TSdk_H}R_{eq}^2\,(d - R_{eq})\frac{R_{eq} - R_m}{R_m}, \tag{A.18}$$

in the exponent in Eq. (A.17) is (strictly) positive. If it is negative, the initial perturbation ρ_0 grows unboundedly with time.

As all parameters in the first factor on the right-hand side of Eq. (A.18) are positive and as the relations $R_{eq} > 0$ and $d > R_{eq}$ are valid by assumption, the sign of Eq. (A.18) depends on the signs of R_m and of the difference $R_{eq} - R_m$. The results are given in the following table (the "case-labels" refer to table (18))

Unstable equilibrium : $\rho(t) \to \infty$ if $R_m < 0$ (case 2),

$$\rho(t) \to \infty \quad \text{if} \quad R_m > 0$$
$$\text{and} \quad R_{eq} < R_m \quad \text{(case 4)}.$$

Stable equilibrium : $\rho(t) \to 0$ if $R_m > 0$

$$\text{and} \quad R_{eq} > R_m \quad \text{(case 3)} \tag{A.19}$$

A.4. Diffusion equation and diffusion current $I(l)$ in an axisymmetric situation

In order to calculate $I(l)$ we first have to solve the diffusion equation in the area where transport of gas particles via diffusion occurs. For the sake of simplicity, we rely on the following assumptions and approximations (see Fig. 26):

(i) No gas particles diffuse across the walls of the pit and of the pit channel.

(ii) Diffusional transport of gas particles through xylem sap is restricted to the embolized side of the pit (that is, the pit membrane is supposed to be dense).

(iii) At a distance $z = z_- := -D$ from the pit and beyond (i.e. for $z \leqslant z_-$) the concentration of dissolved gas particles in the liquid is kept constant at the value $C_D = p_D k_H$.

(iv) The gas/liquid interface at position l coincides approximately with a section of a (fictitious) sphere of radius $r = r_+ := (s/\sin\alpha) - l$ (for $\theta = \pi/2$ the coincidence is exact).

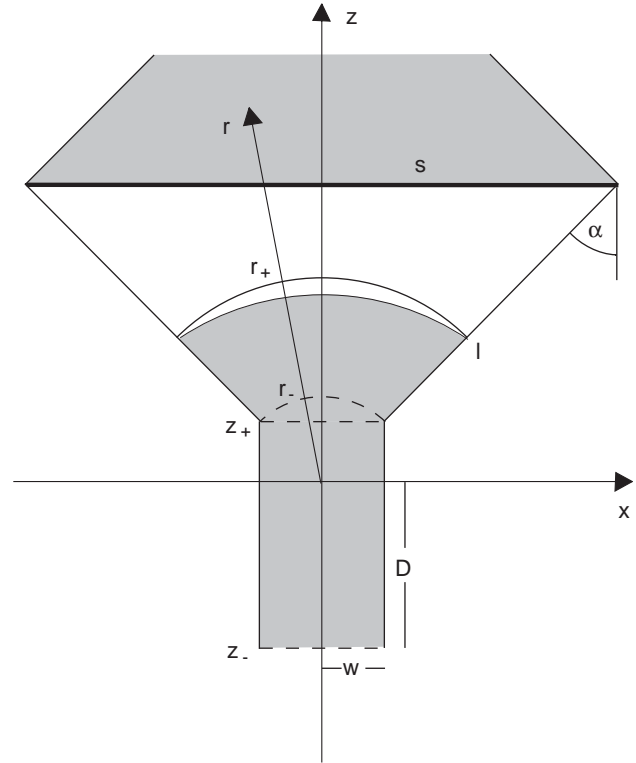(v) The section of a (fictitious) sphere of radius $r = r_- := w/\sin\alpha$ coincides in an approximate sense

Fig. 26. Coordinates used in Section A.4. The z-axis is axis of symmetry. The origin of the coordinate system is at the (fictitious) tip of the pit cone. Thus, the spherical surfaces defined by $r = r_-$ and r_+ intersect the pit cone at right angles. The gas/liquid interface (characterized by l) is also a section of a sphere, but of radius R (as defined in Eq. (19), R is not shown here). Its centre coincides with the origin of the coordinate system only in the special case $\theta = \pi/2$. For $\theta < \pi/2$ it is on the negative, for $\theta > \pi/2$ on the positive part of the z-axis, respectively.

Diffusional currents connect the gaseous space (white) and the plane $z = z_-$, on which the air concentration C_D is held constant.

gray: water, l: position of the gas/liquid interface, s: radius of pit membrane, θ: contact angle, α: pit opening half angle, w: radius of pit neck, D: length of pit channel.

with the (equally fictitious) flat(!), circular disc of radius w at $z = z_+ := w \cot\alpha$.

Thus, we employ a similar auxiliary construction as above, which allows us to work with (i) one-dimensional versions of the diffusion equation (and hence simple, analytic solutions) on two spatial "patches", and (ii) very simple boundary conditions. On the patch defined by $r_- \leqslant r \leqslant r_+$ the time-independent diffusion equation for spherical symmetry reads as

$$\frac{1}{r^2}\frac{d}{dr}\left(r^2\frac{dC}{dr}\right) = 0, \tag{A.20}$$

with general solution

$$C(r) = a + \frac{b}{r}. \tag{A.21}$$

On the patch with $z_- \leqslant z \leqslant z_+$ the cylinder symmetric equivalent of Eq. (A.20) is

$$\frac{\mathrm{d}^2 C}{\mathrm{d}z^2} = 0, \tag{A.22}$$

with solution

$$C(z) = A + Bz. \tag{A.23}$$

a, b, A and B are arbitrary constants which are calculated from the boundary conditions

$$C(r_+) \approx C_l \quad \text{and} \quad C(z_-) = C_D, \tag{A.24}$$

and the conditions of continuity for particle concentration and particle current

$$C(r_-) \approx C(z_+) \quad \text{and} \quad I(r_-) \approx I(z_+). \tag{A.25}$$

Eqs. (A.24) and (A.25) are the formalized versions of assumptions (iii)–(v). Assumption (ii) ("no-flow boundary") is automatically fulfilled by Eqs. (A.21) and (A.23). Application of Eqs. (A.24) and (A.25) to the general solutions (A.21) and (A.23), use of Henry's Law

$$C_l = p k_H, \tag{A.26}$$

and Fick's Law

$$\vec{j} = -S \, grad \, C, \tag{A.27}$$

and an integration similar to that leading from Eq. (A.16) to Eq. (A.17) results in

$$I(l) = 2\pi S k_H w^2 \sin\alpha$$
$$\frac{(s - l\sin\alpha)(p_e - p_D) + 2\gamma\cos(\alpha + \theta)}{(s - l\sin\alpha)[w(1 + 3\cos\alpha) + 2D\sin\alpha] - w^2(1 + \cos\alpha)}. \tag{A.28}$$

References

Cochard, H., Ewers, F., Tyree, M.T., 1994. Water relations of a tropical vinelike bamboo (*Rhipidocladum racemiflorum*): root pressures, vulnerability to cavitation and seasonal changes in embolism. J. Exp. Bot. 45, 1085–1089.

Ewers, F.W., Fisher, J.B., Fichtner, K., 1991. Water flux and xylem structure in vines. In: Putz, F.E. and Mooney, H.A. (Eds), The Biology of Vines. Cambridge University Press, Cambridge.

Hacke, U.G., Stiller, V., Sperry, J.S., Pittermann, J., McCulloh, K., 2001. Cavitation fatigue: embolism and refilling cycles can weaken the cavitation resistance of xylem. Plant Physiol. 125, 779–786.

Holbrook, N.M., Zwieniecki, M.A., 1999. Embolism repair and xylem tension. Do we need a miracle? Plant Physiol. 120, 7–10.

Holbrook, N.M., Burns, M.J., Field, C.B., 1995. Negative xylem pressure in plants: a test of the balancing pressure technique. Science 270, 1193–1194.

Holbrook, N.M., Ahrens, E.T., Burns, M.J., Zwieniecki, M.A., 2001. In vivo observation of cavitation and embolism repair using magnetic resonance imaging. Plant Physiol. 126, 27–31.

van Ieperen, W., Nijsse, J., Keijzer, C.J., van Meeteren, U., 2001. Induction of air embolism in xylem conduits of pre-defined diameter. J. Exp. Bot. 358, 981–991.

Magnani, F., Borghetti, M., 1995. Interpretation of seasonal changes of xylem embolism and plant hydraulic resistance. Plant Cell Environ. 18, 689–696.

McCully, M.E., 1999. Root xylem embolisms and refilling. Relation to water potentials of soil, root and leaves, and osmotic potentials of root xylem sap. Plant Physiol. 119, 1001–1008.

Milburn, J.A., 1991. Cavitation and embolisms in xylem conduits. In: Raghavendra, A.S. (Ed.), Physiology of Trees. Wiley, New York, pp. 163–174.

Pickard, W.F., 1981. The ascent of sap in plants. Prog. Biophys. Molec. Biol. 37, 181–229.

Pockman, W.T., Sperry, J.S., OLeary, J.W., 1995. Sustained and significant negative water pressure in xylem. Nature 378, 715–716.

Salleo, S., LoGullo, M., Depaoli, M., Zippo, M., 1996. Xylem recovery from cavitation-induced embolism in young plants of Laurus nobilis: a possible mechanism. New Phytol. 132, 47–56.

Sperry, J.S., Tyree, M.T., 1988. Mechanism of water stress-induced xylem embolism. Plant Physiol. 88, 581–587.

Sperry, J.S., Donnelly, J.R., Tyree, M.T., 1988. Seasonal occurrence of xylem embolism in sugar maple (*Acer saccharum*). Am. J. Bot. 75, 1212–1218.

Sperry, J.S., Saliendra, N.Z., Pockman, W.T., Cochard, H., Cruiziat, P., Davis, D., Ewers, F.W., Tyree, M.T., 1996. New evidence for large negative xylem pressures and their measurement by the pressure chamber method. Plant Cell Environ. 19, 427–436.

Steudle, E., 2001. The cohesion–tension mechanism and the acquisition of water by plant roots. Annu. Rev. Plant Physiol. Plant Mol. Biol. 52, 847–875.

Tyree, M.T., Ewers, F., 1991. The hydraulic architecture of trees and other woody plants. New Phytol. 199, 345–360.

Tyree, M.T., Sperry, J.S., 1989. Vulnerability of xylem to cavitation and embolism. Annu. Rev. Plant Physiol. Plant Mol. Biol. 40, 19–38.

Tyree, M.T., Yang, S., 1990. Water-storage capacity of Thuja, Tsuga and Acer stems measured by dehydration isotherms: the contribution of capillary water and cavitation. Planta 182, 420–426.

Tyree, M.T., Salleo, S., Nardini, A., LoGullo, M.A., Mosca, R., 1999. Refilling of embolized vessels in young stems of laurel: do we need a new paradigm? Plant Physiol. 120, 11–21.

Yang, S., Tyree, M.T., 1992. A theoretical model of hydraulic conductivity recovery from embolism with comparison to experimental data on Acer saccharum. Plant Cell Environ. 15, 633–643.

Zimmermann, M.H., 1983. Xylem Structure and the Ascent of Sap. Springer, Berlin.

Zwieniecki, M.A., Holbrook, N.M., 2000. Bordered pit structure and vessel wall surface properties. Implications for embolism repair. Plant Physiol. 123, 1015–1020.